Journal of Computational Physics **181,** 354–393 (2002)
doi:10.1006/jcph.2002.7130

Artificial Wind—A New Framework to Construct Simple and Efficient Upwind Shock-Capturing Schemes

Igor' V. Sokolov,*[,1] Eugene V. Timofeev,† Jun-ichi Sakai,* and Kazuyoshi Takayama†

*Laboratory for Plasma Astrophysics, Faculty of Engineering, Toyama University, 3190 Gofuku, Toyama 930-8555, Japan; and †Shock Wave Research Center, Institute of Fluid Science, Tohoku University, 2-1-1 Katahira, Aoba-ku, Sendai 980-8577, Japan
E-mail: igorsok@engin.umich.edu and timo@ceres.ifs.tohoku.ac.jp

Received June 27, 2001; revised January 10, 2002

Using a concept of *artificial wind* having its roots in the Galilean invariance of hydrodynamic equations, we propose a new framework to design upwind shock-capturing schemes. Its application results in simple, efficient, and accurate schemes retaining their simplicity for a broad range of hydrodynamic problems. The global, local, and differential artificial wind approaches are subsequently elaborated. Test results demonstrate efficiency and accuracy of the new schemes in comparison with the Godunov scheme and its second-order extension. The relationship between the artificial wind approach and some existing schemes is also discussed.

Key Words: shock capturing; upwind schemes; Galilean invariance; artificial wind.

1. INTRODUCTION

Many numerical schemes for the hydrodynamic equations as well as for other hyperbolic systems of conservation laws employ to some extent an idea of upwinding. The numerical flux via a face between two adjacent cells should be decomposed into the sum of perturbations propagating across the face in one direction and those propagating in the opposite direction, and numerical differences should be taken accordingly. This approach, based on reasonable physical arguments, is widely used and usually leads to high-quality numerical results.

However, a few circumstances overshadow its application. First of all, for nonlinear equations, such as the hydrodynamic ones, the practical construction of upwind numerical

[1] Present address: Space Physics Research Laboratory, the University of Michigan, Ann Arbor, MI 48109-2143.

0021-9991/02 $35.00

schemes (i.e., procedures to separate the perturbations) is typically accompanied by many technical difficulties that need to be overcome, thus resulting in sophisticated algorithms. For specific implementations of the upwinding approach it may be necessary, for instance, to find the Roe matrix and the total set of its eigenvectors and eigenvalues, to calculate exact or approximate solutions of the Riemann problem, or to apply flux-splitting procedures. Second, these tasks become even more sophisticated for complex physical problems in which, for instance, the effects of real fluids with complex equations of state, equilibrium/nonequilibrium chemistry and thermodynamics, magnetohydrodynamics, special relativity, and so forth, should be taken into account. In some cases the formulas for explicit calculations occupy literally several journal pages requiring tedious programming and reducing computational efficiency. In a specific example of magnetohydrodynamics, an exact Riemann solver is too multivariant due to the multitude of eigenvalues and can hardly be used in practice, while a faithful generalization of the Roe technique is possible only in some particular cases [1]. Finally, each particular physical model may require new generalization of an upwind scheme and, thus, very substantial modifications of existing codes. That is why alternative ways should be sought that would allow the high-quality results typical for upwind schemes while being universal and not so complicated.

Among the upwind schemes developed in the past, the HLL approach [2] is worth mentioning. The HLL scheme is an approximate Riemann solver assuming a wave configuration that consists of two or three waves separating constant states. The numerical flux then can be written in a simple and general form using the wave velocities. However, many authors [3–5], using different reasons, suggest rather complex procedures (based, again, on the Roe solution, etc.) to determine the wave velocities, thus somewhat impairing generality and simplicity.

In [6] we for the first time noticed that the "technological complexity" of the upwinding problem is not Galilean invariant while the hydrodynamic equations are certainly Galilean invariant, and that the Galilean invariance may be effectively exploited to facilitate upwinding in numerical integration of the equations. In [6] and a subsequent publication [7] a new way for constructing simple upwind shock-capturing schemes based on the concept of artificial wind (AW) was proposed. The basic idea is to solve the governing equations in different steadily moving frames of reference chosen in such a way that the flow would be supersonic, resulting in simple upwind formulas for fluxes across control volume faces. An extra velocity (artificial wind) is added to the velocity of the flow under simulation when the system of coordinates is changed. Depending upon how the velocity values are assigned, the global and local artificial wind schemes were proposed in [7]. As was demonstrated in [6, 7], the approach, being very general, allows not only derivations of new schemes but also new interpretations or simplified versions of some already existing schemes.

The present paper is devoted to the systematic description and further application of the artificial wind approach to the development of upwind schemes. In Section 2 we explain our key point—the concept of artificial wind and different ways of practical implementation. Section 3 describes the global and local artificial wind techniques using an approach more transparent and unified than that originally employed in [7]. The differential artificial wind scheme, a newly proposed and superior technique, is introduced in Section 4 while Section 5 examines its relationship with the Godunov scheme. In Section 6 we show how to incorporate a discontinuity, and in particular a contact discontinuity, into the integration path of the differential AW scheme. The second-order and multidimensional extensions of our schemes appear in Section 7, with the results being compared with those for a second-order extension

of the Godunov scheme. Section 8, just prior to Conclusions, briefly outlines the applications of the proposed schemes to the problems of magnetohydrodynamics, special relativity, and compression wave phenomena in water. Some proofs, which are important but not directly needed in the main body of the text, as well as details on the test problem system used in our study are relegated to appendices.

2. ARTIFICIAL WIND CONCEPT

Our main idea for the design of upwind schemes is to avoid entirely the splitting of perturbations, the key and most cumbersome part of any upwind scheme, by making all of them propagate in the same direction, dependent on our choice, and, thus, eradicating all complexities of upwind flux construction. The very possibility of this technique has its roots in the Galilean invariance property of hydrodynamic equations, which stipulates that they retain the same form in all frames of reference moving with a constant speed relative to each other, and that all such systems of coordinates be equally qualified for solving the equations.[2]

There are a few practical ways to implement the idea, all dealing with the introduction of an additional velocity called "artificial wind." As becomes obvious below, all the ways are interrelated and physically equivalent; however they may result in different numerical schemes.

The first, most straightforward way is to change the frame of reference in which the problem under study is being considered. Generally speaking, the frame of reference may be changed from one time integration step to another, even during one time step, such as, for instance, between the predictor and corrector calculations of a numerical scheme. It is always possible to choose a frame of reference which moves with a velocity D with respect to the original frame of reference in such a way that all the flow under consideration becomes supersonic in the new frame. Velocity values in the moving frame of reference are obtained from those in the original one by adding an extra velocity $-D$. We refer to this velocity as an artificial wind (AW) velocity in order to emphasize the fact that its value is a matter of our choice and that it is introduced to facilitate upwinding. The problem of upwinding becomes trivial in the moving frame of reference because in supersonic flows all perturbations propagate along one definite direction depending upon the direction of the AW velocity.[3] The procedure for "remapping" a numerical solution from the moving frame of reference to the original one may be arranged in several ways, for instance by using artificial wind of opposite directions consecutively (see [7], where we applied such an approach to simplify a general second-order predictor–corrector upwind scheme based on flux extrapolation).

There is a certain degree of correlation (more technical than ideological) between the above approach and the widely known Lagrange-remap techniques involving a Lagrangian step (i.e., a finite-difference approximation in Lagrange coordinates) followed by a "remap" step transforming the results of the first step back into the fixed Eulerian grid (see, for instance, [9], among many other papers).

[2] As is pointed out in [8], when considering relativistic hydrodynamics we can also use different moving frames of reference based on the Lorentz invariance of the respective equations.

[3] One may not actually need to add the velocity $-D$ to the original flow velocity transforming the conserved variables $\mathbf{U}$ to their values in the new frame of reference. Alternatively, as follows from simple transformations of the governing equations, it is possible just to modify the expression for gasdynamical fluxes $\mathbf{F}: \mathbf{F} \to \mathbf{F} - D\mathbf{U}$ (see [7]).

The second way to guide all perturbations along one direction is to move control volume faces (during a time step) in such a way that the flow under consideration would become supersonic with respect to the moving faces, and upwind fluxes can be easily calculated using left or right gas dynamic values depending upon the direction of the supersonic flow. In such a case the face velocities represent, in fact, artificial wind velocities. This immediately suggests a potentially useful opportunity to vary the law of face movement from face to face. The approach was mentioned in [7, 10, 11] and is further elaborated here in Section 3 to derive the global and local artificial wind schemes.

Instead of using a moving frame of reference or control volume face one may consider a spatial–temporal invariance of an arbitrary hyperbolic system of conservation laws,

$$\frac{\partial \mathbf{U}}{\partial t} + \frac{\partial \mathbf{F}}{\partial x} = 0, \tag{1}$$

where $\mathbf{U}$ is the vector of conserved variables, $\mathbf{F}$ is the vector of their fluxes, t is time and x is a spatial coordinate (for the sake of simplicity we consider here 1D cases only, without loss of generality). The equations are obviously invariant with respect to the transformation of time and space $t' = t$, $x' = x - Dt$, involving the artificial wind velocity $-D$, as long as the fluxes are also transformed as follows:

$$\mathbf{F}' = \mathbf{F} - D\mathbf{U}. \tag{2}$$

Under this transformation the Jacobian matrix $\mathbf{A} = \partial \mathbf{F}/\partial \mathbf{U}$ becomes

$$\mathbf{A}' = \mathbf{A} - D\mathbf{E}, \tag{3}$$

with $\mathbf{E}$ being the unit matrix, and suffers the shift of all eigenvalues, with the value of the shift being the same for all eigenvalues and equal to the AW velocity $-D$. The physical meaning of the eigenvalues of the Jacobian matrix is that they are the velocities of normal modes of perturbations. Thus, all perturbations may be converted into those moving in the positive direction of the x-axis (all eigenvalues of the Jacobian matrix become positive) or into those moving in the negative direction of the x-axis (if all eigenvalues of the Jacobian matrix become negative) using solely the AW transformation (3). This approach underlies the differential AW scheme elaborated in Section 4.

3. GLOBAL AND LOCAL ARTIFICIAL WIND SCHEMES

Let us consider a one-dimensional time-dependent hyperbolic system of conservation laws. Its integral form for any domain V in x-t space is

$$\oint [\mathbf{U}\,\mathrm{d}x - \mathbf{F}(\mathbf{U})\,\mathrm{d}t] = 0, \tag{4}$$

where the integration is performed along the boundary of the domain in a counter clockwise manner. If the control volume is a rectangle $[x_L, x_R] \times [t_1, t_2]$ the above equation can be obviously written as

$$\int_{x_L}^{x_R} \mathbf{U}(x, t_2)\,\mathrm{d}x = \int_{x_L}^{x_R} \mathbf{U}(x, t_1)\,\mathrm{d}x + \int_{t_1}^{t_2} \mathbf{F}(\mathbf{U}(x_L, t))\,\mathrm{d}t - \int_{t_1}^{t_2} \mathbf{F}(\mathbf{U}(x_R, t))\,\mathrm{d}t. \tag{5}$$

When constructing a numerical scheme, it is usually assumed that $t_1 = t^n$ and $t_2 = t^{n+1}$, with the index n denoting time step numbers (the time step $\Delta t = t^{n+1} - t^n$), while $x_L = x_{i-1/2}$

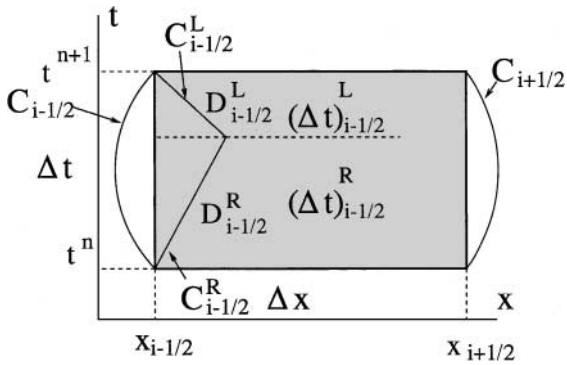

FIG. 1. A control volume in x-t plane.

and $x_R = x_{i+1/2}$ are the left and right faces of the control volume i (the grid step $\Delta x = x_{i+1/2} - x_{i-1/2}$) (see Fig. 1). Following a standard finite-volume procedure and defining cell averages $\mathbf{U}_i^n$, $\mathbf{U}_i^{n+1}$, one may have

$$\mathbf{U}_i^{n+1}\Delta x = \mathbf{U}_i^n \Delta x + \int_{t^n}^{t^{n+1}} \mathbf{F}\big(\mathbf{U}\big(x_{i-1/2}, t\big)\big)\,\mathrm{d}t - \int_{t^n}^{t^{n+1}} \mathbf{F}\big(\mathbf{U}\big(x_{i+1/2}, t\big)\big)\,\mathrm{d}t. \tag{6}$$

The above time integrals are essentially the fluxes across the control volume's faces. The way to compute them is the essence of one or another numerical scheme. For instance, having computed the fluxes using an exact Riemann solver one may get the Godunov scheme.

An important statement should be then made: It is not imperative to perform the time integrations along the vertical lines $x = x_{i-1/2}$ and $x = x_{i+1/2}$. They can be done using virtually any path C (see Fig. 1) connecting, for instance, points $(x_{i-1/2}, t^n)$ and $(x_{i-1/2}, t^{n+1})$. In other words, the above-mentioned control volume V in x-t plane may have a fairly complex shape, with the upper and lower boundaries being straight lines (see Fig. 1) while the left and right boundaries are almost arbitrary curves.[4] Thus, instead of (6) we would have

$$\mathbf{U}_i^{n+1}\Delta x = \mathbf{U}_i^n \Delta x + \int_{C_{i+1/2}} [\mathbf{U}\,\mathrm{d}x - \mathbf{F}(\mathbf{U})\,\mathrm{d}t] - \int_{C_{i-1/2}} [\mathbf{U}\,\mathrm{d}x - \mathbf{F}(\mathbf{U})\,\mathrm{d}t]. \tag{7}$$

It is natural to determine integration paths $C_{i-1/2}$ and $C_{i+1/2}$, from which some advantage could be taken to facilitate the computation of the integrals, for instance to ensure the simplest possible upwinding. This is actually what the artificial wind concept is all about and the flux transformation (2) is in fact equivalent to the application of arbitrary integration paths in (7).

Let us consider the integration path $C_{i-1/2}$, consisting of two straight lines, $C^R_{i-1/2}$ and $C^L_{i-1/2}$ (Fig. 1). Since the lines are on the x-t plane, their slopes are actually velocities $D^R_{i-1/2}$ and $D^L_{i-1/2}$ (artificial wind velocities from here on). Our integration path must arrive

[4] To simplify all considerations of the present and subsequent sections without loss of generality we suppose that all faces may be considered independently; i.e., the integration paths C for different faces do not intersect each other. This can always be achieved by assigning sufficiently small time step values Δt. The stability analysis which follows shows that in fact larger time steps can be used. This is rather similar to the practice commonly employed to derive, for instance, the Godunov and related schemes and to establish their stability conditions [5].

at the point $(x_{i-1/2}, t^{n+1})$, so that the total shift along the t-axis must equal Δt while the total shift along the x-axis must equal 0; i.e.,

$$(\Delta t)^L_{i-1/2} + (\Delta t)^R_{i-1/2} = \Delta t, \tag{8a}$$

$$D^R_{i-1/2}(\Delta t)^R_{i-1/2} + D^L_{i-1/2}(\Delta t)^L_{i-1/2} = 0, \tag{8b}$$

where $\Delta t^R_{i-1/2}$ and $\Delta t^L_{i-1/2}$ are the time intervals during which the face moves with the respective AW velocities.

Let ξ^* be $(\Delta t)^R_{i-1/2}/\Delta t$ $(0 \le \xi^* \le 1)$. The AW velocities should then satisfy the following equality:

$$D^R_{i-1/2}\xi^* = -D^L_{i-1/2}(1-\xi^*). \tag{9}$$

This is the only constraint on their values which stems from the conditions (8a), (8b) for the total spatial and temporal displacement of the control volume face (Fig. 1). It implies, in particular, that $D^R_{i-1/2}$ and $D^L_{i-1/2}$ cannot be both positive or both negative. For convenience, we assume that the AW velocities never equal zero simultaneously. If one of them is zero, another is not, while the equality (9) is satisfied via $\xi^* = 0$ or $\xi^* = 1$; i.e., the nonzero velocity is not actually applied. Under such assumption, without loss of generality, $D^R_{i-1/2} - D^L_{i-1/2} \neq 0$. From (9) it immediately follows that

$$\xi^* = -D^L_{i-1/2}\big/\big(D^R_{i-1/2} - D^L_{i-1/2}\big). \tag{10}$$

Then we may choose the velocity value $D^R_{i-1/2}$ in such a way that it would be not less than the highest speed of disturbance propagation for the control volumes i and $i-1$ and the velocity value $D^L_{i-1/2}$ in such a way that it would be not greater than the lowest speed of disturbance propagation for the same control volumes. We also have to ensure that $D^R_{i-1/2}$ and $D^L_{i-1/2}$ would not be both positive or negative, as follows from the equality (9). All the above conditions are satisfied if

$$D^R_{i-1/2} \ge D^R_{\lim} = \max\{u_{i-1} + c_{i-1}, u_i + c_i, 0\}, \tag{11a}$$

$$D^L_{i-1/2} \le D^L_{\lim} = \min\{u_{i-1} - c_{i-1}, u_i - c_i, 0\}, \tag{11b}$$

where u_i is the gas velocity in the cell i, and c_i is the velocity of sound there. Obviously, we have $D^L_{i-1/2} \le 0 \le D^R_{i-1/2}$.

Let us remark here that for the sake of more transparent explanations we write $u - c$ and $u + c$ in (11a) and (11b) although strictly speaking we should put there, as mentioned above, the lowest and highest speeds of disturbance propagation, i.e. the minimum and maximum eigenvalues, which may not necessarily be $u - c$ and $u + c$ for all hyperbolic conservation laws to which the AW approach is applicable.

Thus, we ensure that when moving along the line $C^R_{i-1/2}$ all disturbances come from the right side, while when moving along the line $C^L_{i-1/2}$ all disturbances come from the left side. Therefore, the task of upwinding becomes trivial. Substituting proper upwind values and the time intervals found from (8a), (8b) into the first integral in (7) we eventually arrive at

$$\begin{aligned}\mathbf{F}_{i-1/2} &= -\frac{1}{\Delta t}\int_{C_{i-1/2}} [\mathbf{U}\,\mathrm{d}x - \mathbf{F}(\mathbf{U})\,\mathrm{d}t] \\ &= [\xi^*\mathbf{F}(\mathbf{U}_i) + (1-\xi^*)\mathbf{F}(\mathbf{U}_{i-1})] - d\cdot(\mathbf{U}_i - \mathbf{U}_{i-1}),\end{aligned} \tag{12}$$

where, using (10) and (9),

$$d = -D^R_{i-1/2} D^L_{i-1/2} \big/ \left(D^R_{i-1/2} - D^L_{i-1/2}\right) = \xi^* D^R_{i-1/2} = -D^L_{i-1/2}(1-\xi^*) \qquad (13)$$

and ξ^* is given by (10). Here and hereafter we omit the time level superscipt n in all expressions for fluxes.

The general definition of the AW velocities (11a), (11b) allows us to introduce them for any flows, including supersonic ones, if desired for some reasons. On the other hand, if the flow under consideration is supersonic the problem of upwinding is trivial and artificial wind for such faces may not be introduced at all. Moreover, it may be even undesirable to use it since, as follows from (12), higher AW velocities increase numerical dissipation. It seems logical not to apply artificial wind to fully supersonic flows and to introduce the minimum needed amount otherwise. That can be achieved, for instance, using the limiting AW values in (11a), (11b). Indeed, for the supersonic case one of the limiting AW velocities equals zero, resulting, as follows from (12), in the simple upwind flux formulas $\mathbf{F}_{i-1/2} = \mathbf{F}(\mathbf{U}_i)$ or $\mathbf{F}_{i-1/2} = \mathbf{F}(\mathbf{U}_{i-1})$, depending on the direction of supersonic flow (i.e., the time integration is done along the lines $x = \text{const}$; see Fig. 1).

In (11a), (11b) the AW values at a face are determined by the gas dynamic parameters in the neighboring cells only. Such a scheme, i.e., (12), (13), (10) with the AW velocities (11a), (11b), is called the local artificial wind scheme.

Aiming at simpler formulas, we may also choose the same AW velocities for all faces everywhere over the computational domain for a given time step (i.e., the integration paths are the same for all faces):

$$D^R \geq D^R_{\lim} = \max_i \{u_i + c_i, 0\}, \qquad (14a)$$

$$D^L \leq D^L_{\lim} = \min_i \{u_i - c_i, 0\}. \qquad (14b)$$

The technique, i.e., (12), (13), (10) with the AW velocities (14a), (14b), is called the global artificial wind scheme. The computational simplicity of the global AW scheme comes at the cost of an increase in numerical diffusion: the above application of a constant artificial wind velocity (determined by the conditions at the grid node having the highest speed of disturbance propagation) throughout the entire computational domain is not optimal; at many grid points the additional velocity may be excessive or just unneeded. Besides, the generalization of the approach to curvilinear and unstructured grids is not straightforward.

The linear stability analysis for the global AW scheme leads to the condition for the AW velocities $\Delta t \leq \Delta x / \max\{D^R, -D^L\}$ as well as to the conventional Courant–Friedrichs–Lewy criterion $\Delta t \leq \Delta x / \max_i \{|u_i| + c_i\}$. One may conclude that as long as

$$\max\{D^R, -D^L\} \leq \max_i \{|u_i| + c_i\}, \qquad (15)$$

the addition of the global AW velocities does not influence the stability of scheme (12). That is the case, for instance, for the AW velocities given by the limiting values in (14a), (14b). However, if the above condition (15) does not hold, an additional restriction on the time step arises from the stability condition.

Any values greater than those determined by (11a), (11b) or (14a), (14b) may serve as global or local AW velocities as well, thus providing a wide selection to choose from.

For example, the choice $D^R = -D^L = \Delta x/\Delta t$ in (14a), (14b) leads to the Lax–Friedrichs scheme. Among the schemes which may be obtained via different choices of the local AW velocities are the Rusanov scheme ($D^R_{i-1/2} = -D^L_{i-1/2} = \max\{|u_{i-1}| + c_{i-1}, |u_i| + c_i\}$) as well as a lot of approximate Riemann solvers belonging to the HLL family (see [2–5]). The HLL schemes based on an approximate, two-wave solution of the Riemann problem at the control volume face have the same flux expression (12) as the local AW scheme, while the meaning of D^L and D^R is completely different. Within the HLL concept they are some speed estimates for the two waves. Although some simple estimates, such as (11a), (11b), are also in use, it is generally believed that more complex choices, such as those employing the Roe matrix eigenvalues or others, may lead to more accurate and/or robust schemes [3–5]. However, it should be noted that more complex options immediately compromise the simplicity of the flux (12) and, thus, do not offer any advantages for MHD, relativistic hydrodynamics, and other applications. Besides, as mentioned above, more severe time step limitations may arise from the stability condition, and the scheme may become more dissipative. In contrast, from the AW theoretical standpoint the simple choice of the velocities equal to their limiting values in (11a), (11b) or (14a), (14b) (i.e., the scheme would operate with as low an artificial wind as possible) seems to be an optimal one and any increase is not needed since it only leads to higher numerical diffusion and smaller time steps.

The test results are presented in Figs. 2a–2e (see Appendix A for details of the test problems). The limiting values of the AW velocities are used. One can see that the solution

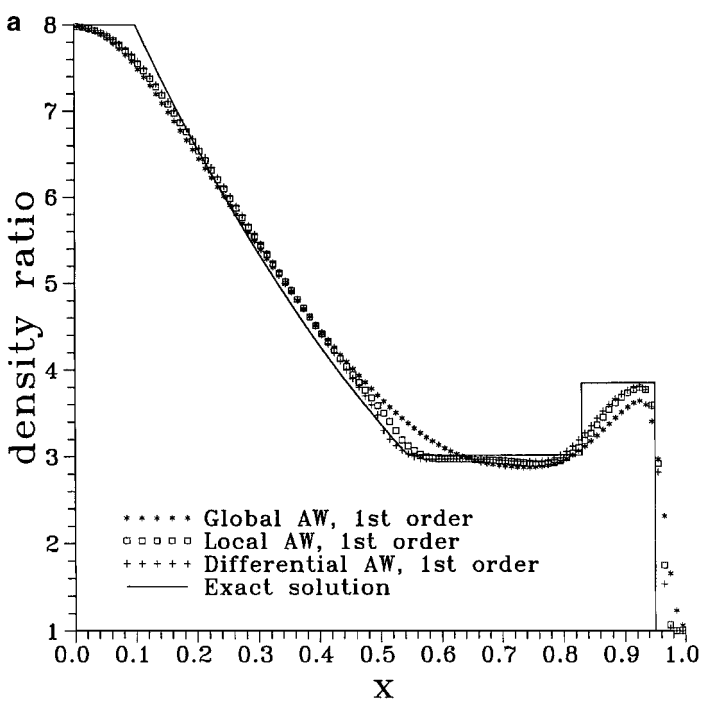

FIG. 2a. Comparison of numerical results with the exact solution of the "480 : 1" test problem ($p_2/p_1 = 480$, $\rho_2/\rho_1 = 8$, $u_2 = u_1 = 0$, $\gamma = 5/3$, 100 grid cells, CFL = 0.8) for the first-order local, global, and differential AW schemes.

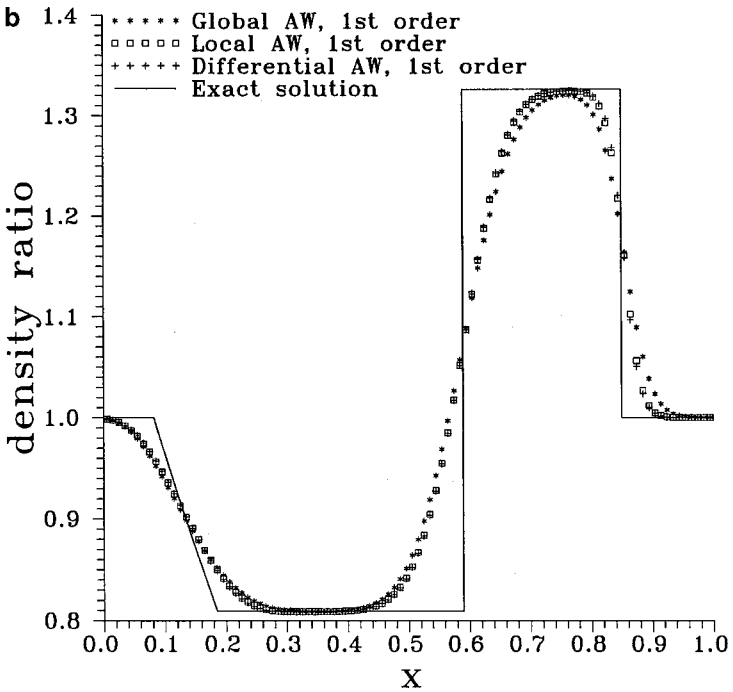

FIG. 2b. Comparison of numerical results with the exact solution of the "2 : 1" test problem ($p_2/p_1 = 2$, $\rho_2/\rho_1 = 1$, $u_2 = u_1 = 0$, $\gamma = 1.4$, 100 grid cells, CFL = 0.8) for the first-order local, global, and differential AW schemes.

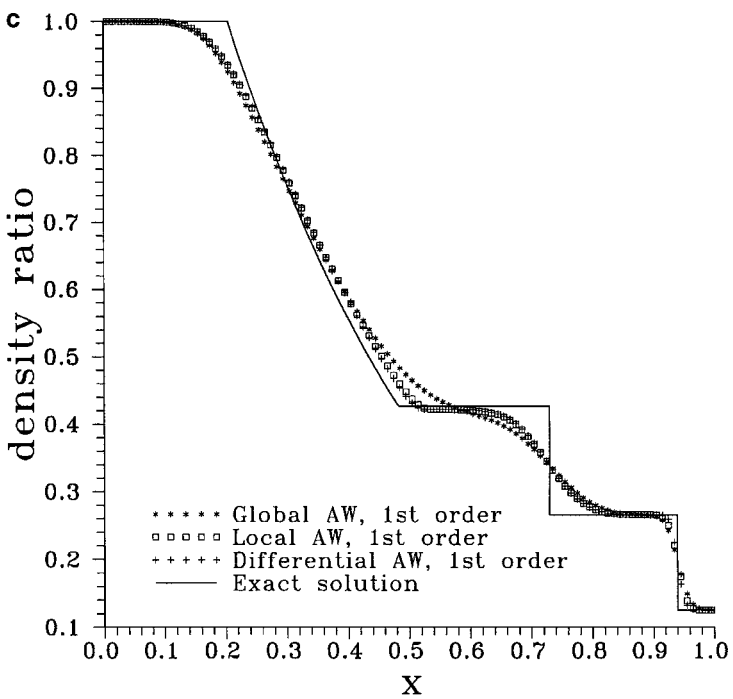

FIG. 2c. Comparison of numerical results with the exact solution of the Sod test problem ($p_2 = 1$, $p_1 = 0.1$, $\rho_2 = 1$, $\rho_1 = 0.125$, $u_2 = u_1 = 0$, $\gamma = 1.4$, 100 grid cells, CFL = 0.8) for the first-order local, global, and differential AW schemes.

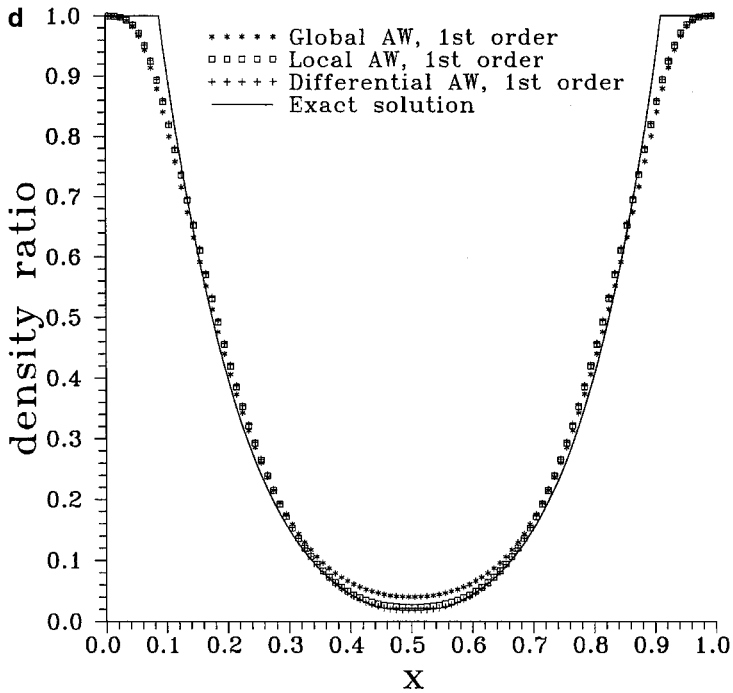

FIG. 2d. Comparison of numerical results with the exact solution of the "vacuum" test problem ($p_2 = p_1 = 0.4$, $\rho_2 = \rho_1 = 1$, $u_2 = -2$, $u_1 = 2$, $\gamma = 1.4$, 100 grid cells, CFL = 0.8) for the first-order local, global, and differential AW schemes.

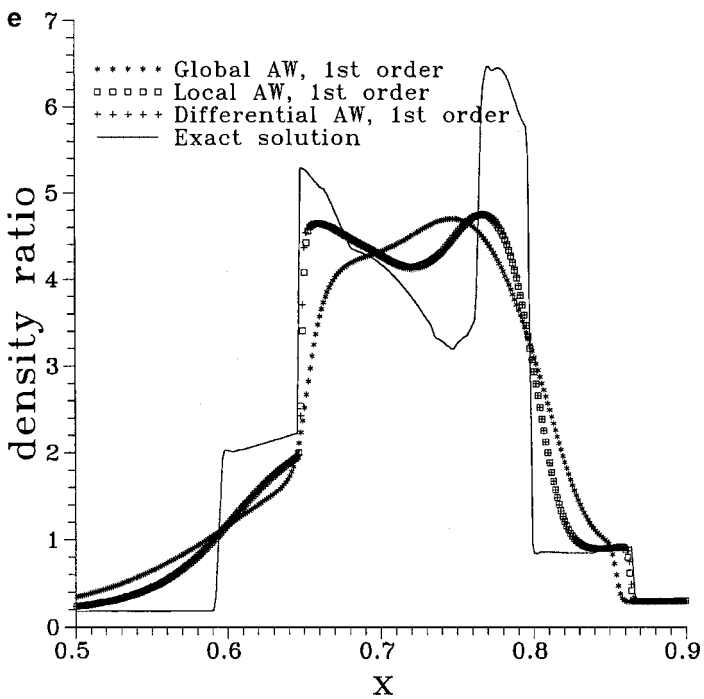

FIG. 2e. Comparison of numerical results with the exact solution of the Woodward and Colella test problem ($\gamma = 1.4$, 800 grid cells, CFL = 0.8) for the first-order local, global, and differential AW schemes.

corresponding to the local AW scheme is more accurate than that of the global AW scheme, thus confirming higher numerical dissipation of the latter.

4. DIFFERENTIAL ARTIFICIAL WIND SCHEME

Comparing the results for the local and global AW schemes one can readily see that the choice of the lowest possible values of AW velocities pays off in less dissipation and better accuracy. The global AW velocities ensuring that the flow is supersonic throughout the computational domain are normally larger than the local AW velocities for a particular face, which ensure supersonic flow only within the cells adjacent to this face. That is why the numerical diffusion of the local AW scheme is lower compared to that of the global AW scheme.

Exploiting the above observation we try here to gain further decrease in the numerical dissipation. We no longer limit AW velocities to values based on the *averaged* conserved variables $\mathbf{U}_{i-1}$ and $\mathbf{U}_i$ for the control volumes $i-1$ and i. Instead, we assign them separately for each of the *intermediate states between* $\mathbf{U}_{i-1}$ and $\mathbf{U}_i$, which may be obtained using linear interpolation with the weight coefficient $\xi (0 \le \xi \le 1)$:

$$\bar{\mathbf{U}}(\xi, \mathbf{U}_{i-1}, \mathbf{U}_i) = \mathbf{U}_{i-1} + \xi \cdot (\mathbf{U}_i - \mathbf{U}_{i-1}) = (1-\xi) \cdot \mathbf{U}_{i-1} + \xi \cdot \mathbf{U}_i. \tag{16}$$

The choice of conserved variables for this interpolation is not compulsory. One can use primitive variables, pseudocharacteristic ones, or even more complex choices. Such possibilities will be explored elsewhere.

Upon the integration of the Jacobian $\mathbf{A} = \partial \mathbf{F}/\partial \mathbf{U}$ over the intermediate states one can readily find that

$$\mathbf{F}(\mathbf{U}_i) - \mathbf{F}(\mathbf{U}_{i-1}) = \int_0^1 \mathbf{A}(\bar{\mathbf{U}}(\xi))\, \mathrm{d}\xi \cdot (\mathbf{U}_i - \mathbf{U}_{i-1}). \tag{17}$$

The key point here is the formal application of the AW transformation (3) to the Jacobian matrix $\mathbf{A}$ in (17) at each intermediate state ξ, so that the latter equation becomes

$$\mathbf{F}(\mathbf{U}_i) - \mathbf{F}(\mathbf{U}_{i-1}) = \int_0^1 [\mathbf{A}(\bar{\mathbf{U}}(\xi)) - D(\xi)\mathbf{E}]\, \mathrm{d}\xi \cdot (\mathbf{U}_i - \mathbf{U}_{i-1}). \tag{18}$$

To ensure that the equality in (18) still holds, the AW velocity $D(\xi)$ must satisfy the condition

$$\int_0^1 D(\xi)\, \mathrm{d}\xi = 0, \tag{19}$$

which has the same meaning as (8a), (8b) or (9).

Now let us assign the velocity of the *differential* artificial wind as follows. On the interval $\xi \in [0, \xi^*]$ the AW velocity should be nonnegative and not less than the maximum eigenvalue of the Jacobian matrix $\mathbf{A}(\bar{\mathbf{U}}(\xi))$:

$$D(\xi) = D^R(\xi) \ge D^R_{\lim}(\xi) = \max\{0, u(\xi) + c(\xi)\}, \quad \xi \in [0, \xi^*]. \tag{20}$$

Then the integration in (18) between the limits 0 and ξ^*, namely

$$\int_0^{\xi^*} [\mathbf{A}(\bar{\mathbf{U}}(\xi)) - D^R(\xi)\mathbf{E}]\, \mathrm{d}\xi \cdot (\mathbf{U}_i - \mathbf{U}_{i-1}), \tag{21}$$

becomes a sum of perturbations propagating in the negative direction of the x-axis because the transformed Jacobian matrix $\mathbf{A}(\bar{\mathbf{U}}(\xi)) - D(\xi)\mathbf{E}$ has only negative eigenvalues as long as the inequality (20) holds.

Then for the remaining integration interval $\xi \in [\xi^*, 1]$ the AW velocity should be nonpositive and not greater than the minimum eigenvalue of the Jacobian matrix $\mathbf{A}(\bar{\mathbf{U}}(\xi))$:

$$D(\xi) = D^L(\xi) \le D^L_{\lim}(\xi) = \min\{0, u(\xi) - c(\xi)\}, \quad \xi \in [\xi^*, 1]. \tag{22}$$

The integral

$$\int_{\xi^*}^{1} [\mathbf{A}(\bar{\mathbf{U}}(\xi)) - D^L(\xi)\mathbf{E}]\, \mathrm{d}\xi \cdot (\mathbf{U}_i - \mathbf{U}_{i-1}) \tag{23}$$

becomes a sum of perturbations propagating in the positive direction of the x-axis because the transformed Jacobian matrix $\mathbf{A}(\bar{\mathbf{U}}(\xi)) - D(\xi)\mathbf{E}$ has only positive eigenvalues.

The flux difference $\mathbf{F}(\mathbf{U}_i) - \mathbf{F}(\mathbf{U}_{i-1})$ is thus split into the perturbations propagating along the x-axis in opposite directions. Therefore, the problem of upwinding is solved and one can now construct an upwind numerical flux using one of the following equivalent expressions:

$$\begin{aligned} \mathbf{F}_{i-1/2} &= \mathbf{F}_{i-1} + \int_0^{\xi^*} [\mathbf{A}(\bar{\mathbf{U}}(\xi)) - D^R(\xi)\mathbf{E}]\, \mathrm{d}\xi \cdot (\mathbf{U}_i - \mathbf{U}_{i-1}) \\ &= \mathbf{F}_i - \int_{\xi^*}^{1} [\mathbf{A}(\bar{\mathbf{U}}(\xi)) - D^L(\xi)\mathbf{E}]\, \mathrm{d}\xi \cdot (\mathbf{U}_i - \mathbf{U}_{i-1}). \end{aligned} \tag{24}$$

It is pertinent to compare the above formulas with the conventional expressions for a linear upwind scheme or the nonlinear Roe scheme, $\mathbf{F}_{i-1/2} = \mathbf{F}_{i-1} + \mathbf{A}^-(\mathbf{U}_i - \mathbf{U}_{i-1}) = \mathbf{F}_i - \mathbf{A}^+(\mathbf{U}_i - \mathbf{U}_{i-1})$, where $\mathbf{A}^-$ and $\mathbf{A}^+$ are negative and positive parts of the linear Jacobian matrix or nonlinear Roe matrix which correspond to the respective perturbations.

Upon calculation of the integrals (24) one can finally obtain

$$\mathbf{F}_{i-1/2} = \mathbf{F}\{\xi^*\mathbf{U}_i + (1 - \xi^*)\mathbf{U}_{i-1}\} - d \cdot (\mathbf{U}_i - \mathbf{U}_{i-1}), \tag{25}$$

where the diffusion coefficient d is given by either of the two integrals

$$d = \int_0^{\xi^*} D^R(\xi)\, \mathrm{d}\xi = -\int_{\xi^*}^{1} D^L(\xi)\, \mathrm{d}\xi. \tag{26}$$

The equality of the integrals comes from (19).

In case the velocities $D^L(\xi)$ and $D^R(\xi)$ are given, the equality (26) turns into the equation for finding ξ^*. The function $Z(\xi^*) = \int_0^{\xi^*} D^R(\xi)\, \mathrm{d}\xi + \int_{\xi^*}^{1} D^L(\xi)\, \mathrm{d}\xi$ is nonpositive at $\xi^* = 0$ and nonnegative at $\xi^* = 1$; its derivative $Z'_{\xi^*} = D^R(\xi^*) - D^L(\xi^*)$ is positive for $\xi^* \in [0; 1]$. Thus, Eq. (26) has one and only one root (i.e., one and only one value of ξ^* satisfies it).

Generally, to get analytical expressions for ξ^* and d, the integrals (26) should be taken assuming some particular $D^R(\xi)$ and $D^L(\xi)$ satisfying (20), (22) and the resulting equation should be solved. It may not be always possible to perform one or both of the above-mentioned steps analytically or the resulting formulas may be quite cumbersome. Thus, in computational practice it may be reasonable to find ξ^* and d numerically using an iteration

procedure. For instance, we suggest using the simplest trapezoidal approximation (assuming the limiting values of AW velocities in (20), (22)):

$$\tilde{D}^L\left(\xi^{*(k)}\right) = 0.5\left(\min\{u_i - c_i, 0\} + \min\left\{u\left(\xi^{*(k)}\right) - c\left\{\left(\xi^{*(k)}\right), 0\right\}\right\}\right), \tag{27a}$$

$$\tilde{D}^R\left(\xi^{*(k)}\right) = 0.5\left(\max\{u_{i-1} + c_{i-1}, 0\} + \max\left\{u\left(\xi^{*(k)}\right) + c\left\{\left(\xi^{*(k)}\right), 0\right\}\right\}\right), \tag{27b}$$

$$\xi^{*(k+1)} = -\tilde{D}^L\left(\xi^{*(k)}\right)/\left[\tilde{D}^R\left(\xi^{*(k)}\right) - \tilde{D}^L\left(\xi^{*(k)}\right)\right]. \tag{27c}$$

The first approximation $\xi^{*(1)}$ is taken from the local artificial wind formula (10). Upon convergence the diffusion coefficient may be calculated as

$$d = \max\left\{\xi^{*(k+1)}\tilde{D}^R\left(\xi^{*(k+1)}\right), \quad -\left(1 - \xi^{*(k+1)}\right)\tilde{D}^L\left(\xi^{*(k+1)}\right)\right\}. \tag{28}$$

Practical computations reveal that the above iterations have a very high convergence rate: the first iteration leads to ξ^*, which differs from the fully converged value by several tenths of a percent at most. Taking into account the fact that the simplest trapezoidal approximation is used for the integrals (26), we may conclude that additional iterations are not needed. Numerical tests confirm that. Thus, we need only one iteration at most. At some faces (near discontinuities) this iteration is really important and cannot be neglected: it significantly, by up to 30–40%, reduces the diffusion coefficient d. However, in most cases even this first iteration is excessive. As a rule of thumb, the following procedure could be suggested: having an initial approximation for ξ^* the "left" and "right" diffusion coefficients are computed as in the right hand side of (28). In case the difference between them is less than a threshold (a few percent is a good choice), the iterations should not be performed at all. This is not unlike an exact Riemann solver: typically, a full course of iterations should actually be performed only for a small percentage of total nodes.

Let us now compare the differential AW scheme (25), (26), (20), (22) and the local AW scheme (12), (13), (10), (11a), (11b) under the most simple choice of the differential AW velocities: $D^R(\xi) = \text{const}$ and $D^L(\xi) = \text{const}$. Equation (26) becomes identical to (13), and the value of ξ^* for both schemes may be found from (10). One can see that the only difference between the local and differential AW schemes (under the assumption that the differential AW velocities are constant!) is that the local AW scheme deals with the linear combination of fluxes $\xi^*\mathbf{F}(\mathbf{U}_i) + (1 - \xi^*)\mathbf{F}(\mathbf{U}_{i-1})$ while the differential AW scheme computes only one flux at a proper intermediate state: $\mathbf{F}[\xi^*\mathbf{U}_i + (1 - \xi^*)\mathbf{U}_{i-1}]$. From this point of view, the differential AW scheme is more efficient since the hydrodynamic flux should be calculated only once (at the intermediate state) while for the local AW scheme the flux in general cases should be calculated twice (at the left and right states).

Test results for the limiting values of the AW velocities in (20), (22) are shown in Figs. 2a–2e. The solution produced by the differential AW scheme is more accurate and less dissipative compared to that of the local AW scheme. The lowered dissipation even leads to the appearance of a slight kink in the vicinity of the sonic point (test "480 : 1"), which is smeared out by the global and local AW schemes.

Although the differential AW flux is simple enough, a few further practical simplifications are possible. First, we may apply the intermediate state interpolation over the primitive variables $\mathbf{V} = (\rho, u, p)$ in (25),

$$\mathbf{F}_{i-1/2} = \mathbf{F}[\xi^*\mathbf{V}_i + (1 - \xi^*)\mathbf{V}_{i-1}] - d \cdot (\mathbf{U}_i - \mathbf{U}_{i-1}), \tag{29}$$

and in (27a), (27b) to compute $u(\xi^*) \pm c(\xi^*)$. While the modification does not affect the accuracy of numerical results it may be useful for some particular codes since it allows us to economize on the transformations from conserved to primitive variables and vice versa. Second, we may assume that $u + c$ and $u - c$ vary linearly with ξ (that is, the intermediate state interpolation (16) is performed using characteristic variables). The assumption results in a quadratic equation for ξ^*, from which, introducing the notations $D^{LR} = \min\{0, u_i - c_i\}$, $D^{LL} = \min\{0, u_{i-1} - c_{i-1}\}$, $D^{RR} = \max\{0, u_i + c_i\}$, $D^{RL} = \max\{0, u_{i-1} + c_{i-1}\}$ and $\kappa = (D^{RR} - D^{LR})/(D^{RL} - D^{LL})$, $\bar{\kappa} = (D^{LR} + D^{LL})/(D^{RL} - D^{LL})$, we have its explicit expression:

$$\xi^* = \begin{cases} \frac{\sqrt{1-(\kappa-1)\bar{\kappa}}-1}{\kappa-1} & \text{if } \kappa \neq 1, \\ -0.5\bar{\kappa} & \text{if } \kappa = 1. \end{cases} \tag{30}$$

Thus, we avoid iterations altogether. The accuracy of numerical results again varies insignificantly when implementing such an approach.

The comparison with the Godunov scheme is presented in Figs. 3a–3e. One can see that the differential AW scheme provides the results, which are very close to those of the Godunov scheme. The only exception is contact discontinuity: the schemes exhibit basically the same resolution for the 480 : 1, Sod and "vacuum" tests, while for the "2 : 1" test, with the contact discontinuity moving about 20 times slower than its 480 : 1 counterpart, the Godunov scheme performs better. Its superiority in the Woodward and Colella test is also evident. Thus, the tests reveal that the differential AW scheme does not resolve contact

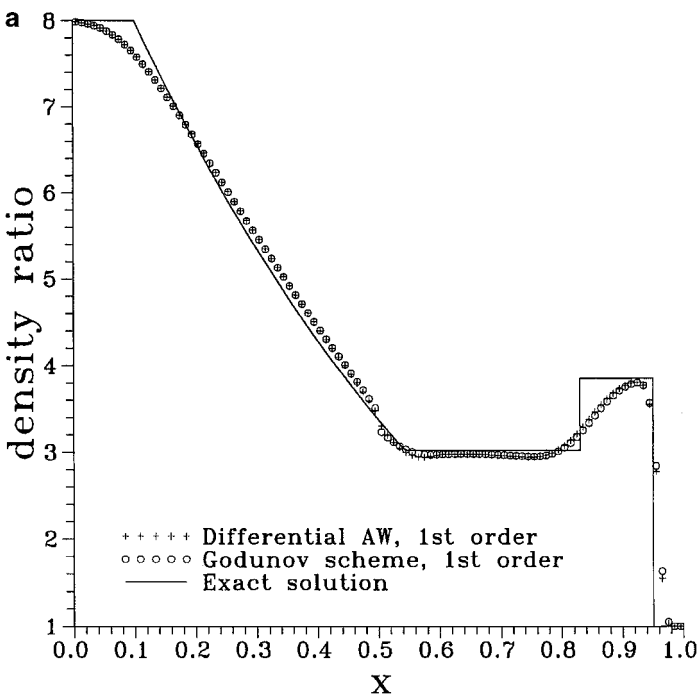

FIG. 3a. Comparison of the first-order differential AW and Godunov schemes using the "480 : 1" test problem ($p_2/p_1 = 480$, $\rho_2/\rho_1 = 8$, $u_2 = u_1 = 0$, $\gamma = 5/3$, 100 grid cells, CFL = 0.8).

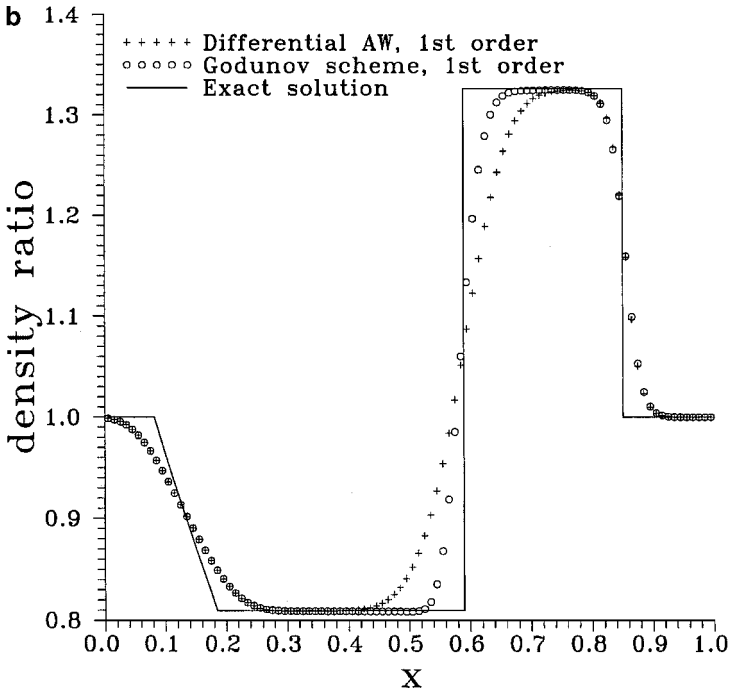

FIG. 3b. Comparison of the first-order differential AW and Godunov schemes using the "2 : 1" test problem ($p_2/p_1 = 2$, $\rho_2/\rho_1 = 1$, $u_2 = u_1 = 0$, $\gamma = 1.4$, 100 grid cells, CFL = 0.8).

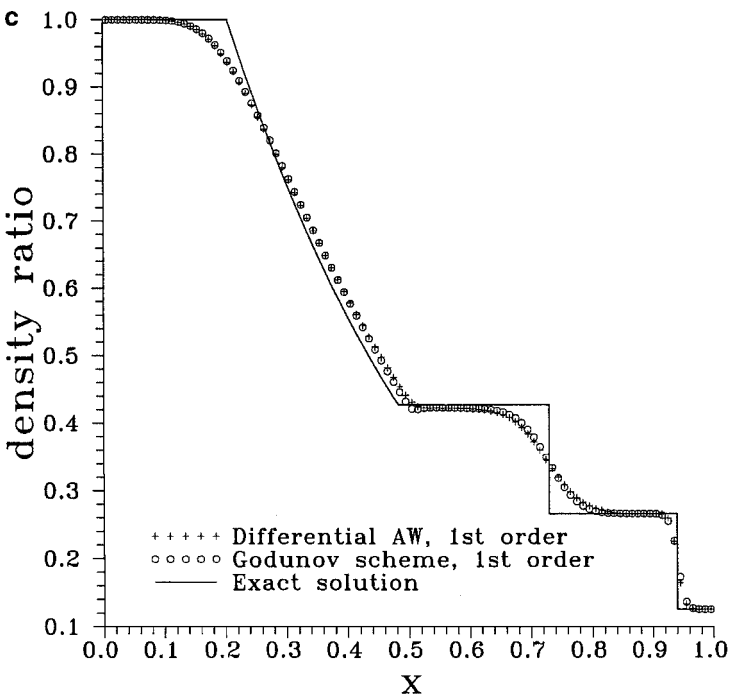

FIG. 3c. Comparison of the first-order differential AW and Godunov schemes using the Sod test problem ($p_2 = 1$, $p_1 = 0.1$, $\rho_2 = 1$, $\rho_1 = 0.125$, $u_2 = u_1 = 0$, $\gamma = 1.4$, 100 grid cells, CFL = 0.8).

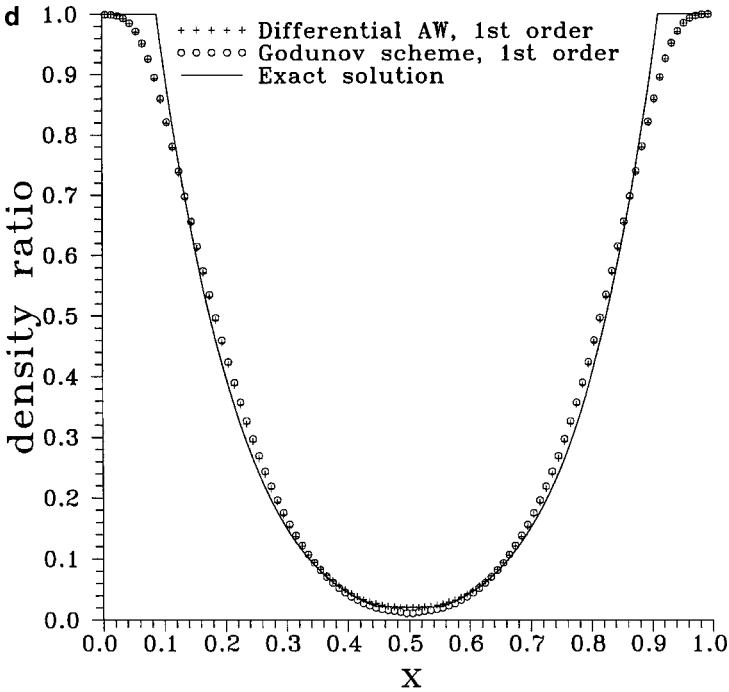

FIG. 3d. Comparison of the first-order differential AW and Godunov schemes using the "vacuum" test problem ($p_2 = p_1 = 0.4$, $\rho_2 = \rho_1 = 1$, $u_2 = -2$, $u_1 = 2$, $\gamma = 1.4$, 100 grid cells, CFL = 0.8).

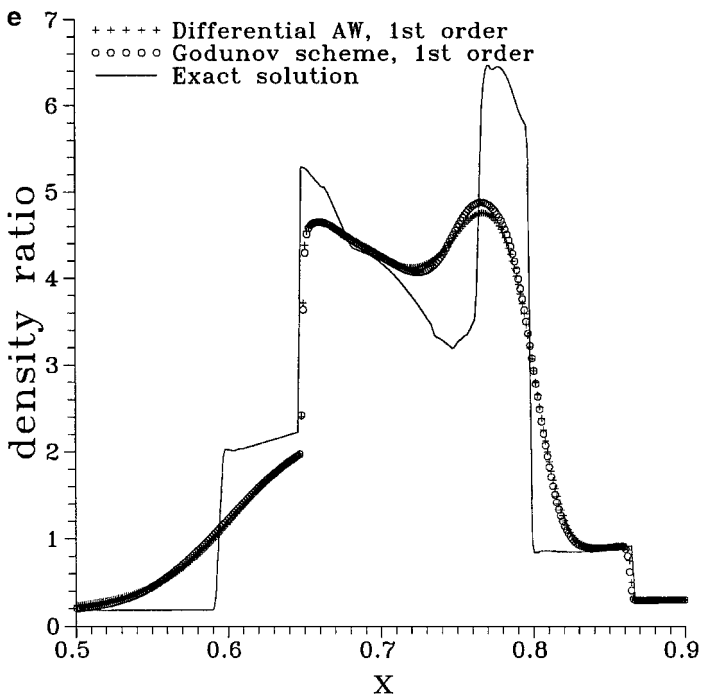

FIG. 3e. Comparison of the first-order differential AW and Godunov schemes using the Woodward and Colella test problem ($\gamma = 1.4$, 800 grid cells, CFL = 0.8).

discontinuities, especially slowly moving ones, as well as the Godunov scheme does (similar to many other upwind schemes; see [5]). The issue will be addressed in detail in Section 6.

5. THE RELATIONSHIP OF THE DIFFERENTIAL AW AND GODUNOV SCHEMES

5.1. The Case of a Nonlinear Scalar Hyperbolic Conservation Law

Let us consider a nonlinear scalar hyperbolic conservation equation $\partial U/\partial t + \partial F/\partial x = 0$ with a convex flux, i.e., $\partial^2 F/\partial U^2 > 0$, and its numerical approximation $(U_i^{n+1} - U_i^n)/\Delta t + (F_{i+1/2}^n - F_{i-1/2}^n)/\Delta x = 0$. We denote $\partial F/\partial U$ as $a(U)$, omitting the superscript n in all flux expressions hereafter.

The Godunov scheme flux for the equation may be found, for instance, in [12]:

$$F_{i-1/2}^G = \begin{cases} \min_{U_{i-1} \le U \le U_i} F(U) & \text{if } U_{i-1} < U_i, \\ \max_{U_{i-1} \ge U \ge U_i} F(U) & \text{if } U_{i-1} > U_i. \end{cases}$$

It turns out that for the case under consideration the numerical flux of the differential AW scheme, with the AW velocities being equal to their limiting values in (20), (22), is identical to that of the Godunov scheme. The proof may be found in Appendix B.

5.2. Differential AW Scheme as a Modification of the Godunov Scheme

The differential AW scheme may be interpreted as a variation of the Godunov scheme, which is also based on the exact solution of the Riemann problem but operates with a modified initial distribution of gas dynamic parameters within computational cells. Although the interpretation does not lead to practically instructive definitions of AW velocities, it clearly demonstrates similarities and differences in the schemes. It is also useful in proving some properties of the differential AW scheme.

Let us recall the basic principles of the Godunov scheme. The first key feature is the assumption of a piecewise constant distribution of the conserved vector **U** at the initial time level n, with discontinuities at intercell boundaries (see Fig. 4). The scheme updating

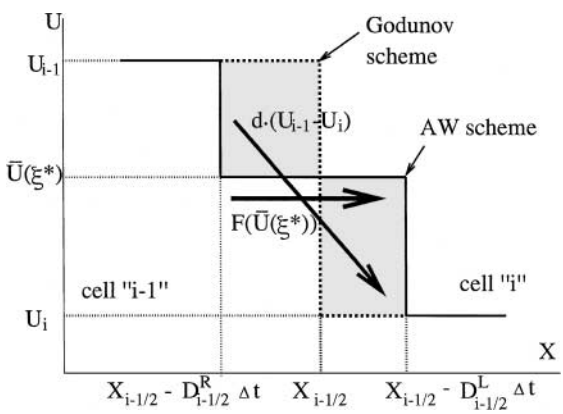

FIG. 4. Schematic of the initial distributions of gas dynamic parameters at a face for the artificial wind (solid line) and Godunov (bold dashed line) schemes. Shaded areas are equal.

the initial distribution over a time step Δt may then be constructed using the system of conservation laws (5) for a control volume in x-t space (see Fig. 1). As was stated in Section 3, the first two integrals in (5) result in the cell averages $\mathbf{U}_i^n$ and $\mathbf{U}_i^{n+1}$, as in (6), which form the above-mentioned piecewise constant distribution. The remaining two integrals are the fluxes $\mathbf{F}_{i-1/2}^n$ and $\mathbf{F}_{i+1/2}^n$ across the control volume's faces, so that we have, omitting the superscript n in flux expressions hereafter,

$$\mathbf{U}_i^{n+1} = \mathbf{U}_i^n - \frac{\Delta t}{\Delta x}\left(\mathbf{F}_{i+1/2} - \mathbf{F}_{i-1/2}\right). \tag{31}$$

The second key feature is that the above fluxes is to be computed using the exact self-similar solutions of the Riemann problems at the respective interfaces $\mathbf{U}_{i-1/2}^{\mathrm{RS}}(\mathbf{U}_{i-1}, \mathbf{U}_i, x/t)$, for instance $\mathbf{F}_{i-1/2}^G = \mathbf{F}(\mathbf{U}_{i-1/2}^{\mathrm{RS}}(\mathbf{U}_{i-1}, \mathbf{U}_i, 0))$.

Now let us modify the piecewise constant distribution of the Godunov scheme, first by introducing two additional interfaces, located at $x_L = x_{i-1/2} - D_{i-1/2}^R \Delta t$ and $x_R = x_{i-1/2} - D_{i-1/2}^L \Delta t$, where $D_{i-1/2}^L$ and $D_{i-1/2}^R$ are some artificial wind velocities. The Godunov piecewise distribution with a discontinuity at $x_{i-1/2}$ is then averaged over the interval $[x_L, x_R]$, resulting in an intermediate state $\bar{\mathbf{U}}(\xi^*)$,

$$\bar{\mathbf{U}}(\xi^*) = \mathbf{U}_i \xi^* + \mathbf{U}_{i-1}(1 - \xi^*), \tag{32}$$

where ξ^* is defined in (10). Thus, a modified initial distribution with two discontinuities, at x_L and x_R, is created (see Fig. 4). Let us require that the AW velocities be "large enough" so that the waves of the exact self-similar solutions of the Riemann problems at x_L and x_R do not reach the face $x_{i-1/2}$ during the time interval Δt. We note that a general subsonic case is considered here.

It is easy to show that the application of the Godunov scheme methodology to the modified three-level initial distribution described above results in the differential AW flux.

Indeed, since the gas dynamic parameters are constant across the face $x_{i-1/2}$ and the waves originating from the discontinuities at x_L and x_R do not reach it, there is no need to actually calculate any exact solutions of the Riemann problems. The flux $\mathbf{F}_{i-1/2}$ is simply determined by the parameters at the intermediate state: $\mathbf{F}_{i-1/2} = \mathbf{F}(\bar{\mathbf{U}}(\xi^*))$.

However, since the Godunov piecewise distribution has been modified, the second integral in (5) no longer produces the cell average $\mathbf{U}_i^n$. Instead, considering only one face without loss of generality we have

$$\frac{1}{\Delta x}\int_{x_{i-1/2}}^{x_{i+1/2}} \mathbf{U}(x, t_n)\,\mathrm{d}x = \mathbf{U}_i^n - \frac{\Delta t}{\Delta x} D_{i-1/2}^L (\bar{\mathbf{U}}(\xi^*) - \mathbf{U}_i) = \mathbf{U}_i^n - \frac{\Delta t}{\Delta x} d \cdot (\mathbf{U}_i - \mathbf{U}_{i-1}), \tag{33}$$

where d is given by (13); the second equality is obtained using (32). From (33), (13), and (32) it also follows that

$$(\mathbf{U}_i - \bar{\mathbf{U}}(\xi^*)) D_{i-1/2}^L = (\mathbf{U}_{i-1} - \bar{\mathbf{U}}(\xi^*)) D_{i-1/2}^R,$$

confirming that the averaging (32) is a conservative procedure (this is graphically represented by the equal shaded areas in Fig. 4).

To stay within the formulation given by (31) we should interpret the second term in (33) as an additional flux across the face originating from the averaging procedure (32) and

include it into $\mathbf{F}_{i-1/2}$, which now becomes

$$\mathbf{F}_{i-1/2} = \mathbf{F}(\bar{\mathbf{U}}(\xi^*)) - d \cdot (\mathbf{U}_i - \mathbf{U}_{i-1}). \tag{34}$$

The numerical flux (34) coincides with that of the differential AW scheme (25) if (see (13) and (26)) the AW velocities are equal to

$$D^L_{i-1/2} = \frac{\int_{\xi^*}^1 D^L(\xi)\,\mathrm{d}\xi}{1-\xi^*}, \quad D^R_{i-1/2} = \frac{\int_0^{\xi^*} D^R(\xi)\,\mathrm{d}\xi}{1-\xi^*}, \tag{35}$$

where $D^L(\xi)$ and $D^R(\xi)$ satisfy (20) and (22), respectively.

The above interpretation allows us to conclude that the differential AW scheme possesses the property of entropy nondecreasing. The averaging (32) is physically equivalent to mixing two hydrodynamic states, obviously not decreasing entropy. From a mathematical point view, the Jensen inequality requires that entropy does not decrease at this averaging (see the proof of an analogous statement in [2]). The scheme is then constructed in the same way as the Godunov one, so the entropy nondecreasing property can be proven as is done in [2] for the Godunov scheme.

6. DIFFERENTIAL AW SCHEME WITH CONTACT DISCONTINUITY

6.1. Preliminary Considerations

The artificial wind methods developed so far belong to the schemes with scalar numerical dissipation in contrast to more sophisticated approaches adjusting the dissipation separately for each characteristic [5, 12]. By definition, the artificial wind velocities are equal (or greater in absolute value) to the maximum and minimum eigenvalues (the highest and lowest speed of disturbance propagation) of a hyperbolic conservation law. It is generally not guaranteed that the magnitude of numerical dissipation would be optimal for all perturbations corresponding to the whole spectrum of the system under consideration.

To illuminate this point let us consider a linear hyperbolic system $\partial\mathbf{U}/\partial t + \mathbf{A}\partial\mathbf{U}/\partial x = 0$, with $\mathbf{A}$ being a diagonal matrix with the constant coefficients a_k; $a_{\min} = \min_k\{a_k\}$, $a_{\max} = \max_k\{a_k\}$. The system describes linear advection with different characteristic velocities a_k. The differential AW flux for the system may be written in the form of two equivalent expressions:

$$\begin{aligned}\mathbf{F}_{i-1/2} &= \mathbf{A}\mathbf{U}_{i-1} - \frac{D^L(\mathbf{A} - D^R\mathbf{E})}{D^R - D^L}(\mathbf{U}_i - \mathbf{U}_{i-1}) \\ &= \mathbf{A}\mathbf{U}_i - \frac{D^R(\mathbf{A} - D^L\mathbf{E})}{D^R - D^L}(\mathbf{U}_i - \mathbf{U}_{i-1}),\end{aligned} \tag{36}$$

with the AW velocities $D^L = \min\{0, a_{\min}\}$ and $D^R = \max\{0, a_{\max}\}$. Each expression consists of a purely upwind numerical flux and an additional dissipative term.

The additional dissipation vanishes if $a_{\min} > 0$ or $a_{\max} < 0$ (the "supersonic" case). For $a_{\min} < 0 < a_{\max}$ it becomes zero only for the perturbations propagating with the maximum or minimum characterestic speeds, i.e., for $a_k = a_{\min}$ or $a_k = a_{\max}$. Thus, for all intermediate characteristic speeds a_k, $a_{\min} < a_k < a_{\max}$, the numerical dissipation of the differential AW scheme is exceeded by the amount proportional to $a_k - a_{\min}$ or $a_k - a_{\max}$.

The above example serves as one possible explanation of the excessive smearing of slowly moving contact discontinuities by the artificial wind schemes demonstrated in the previous section. From another point of view, this drawback stems from the excessive entropy production at the averaging (32) (see Section 5.2). One possible way out of the situation is to partly keep a jump of the conserved variables at the control volume face instead of the full averaging (32). The present section is devoted to the exploration of such an opportunity. First, we formally show how to incorporate a physical discontinuity into the integration path of the differential AW scheme (Section 6.2). Then, we provide a physical interpretation of the procedure (Section 6.3). Finally, the particular case of a contact discontinuity is considered (Section 6.4).

6.2. Incorporation of a Physical Discontinuity

In Section 4 the intermediate states $\bar{\mathbf{U}}(\xi)$ between $\mathbf{U}_{i-1}$ and $\mathbf{U}_i$ were introduced using linear interpolation (see (16)). Let us now include an internal discontinuity at $\xi = \xi^*$; i.e.,

$$\tilde{\mathbf{U}}(\xi) = \begin{cases} \mathbf{U}_{i-1} + \frac{\xi}{\xi^*}(\mathbf{U}_L - \mathbf{U}_{i-1}) & \text{if } 0 \le \xi \le \xi^*, \\ \mathbf{U}_R + \frac{\xi - \xi^*}{1-\xi^*}(\mathbf{U}_i - \mathbf{U}_R) & \text{if } \xi^* \le \xi \le 1, \end{cases} \tag{37}$$

where $\mathbf{U}_L$ and $\mathbf{U}_R$ are the conserved variables on the left and right sides of the discontinuity. We consider here a general subsonic case, so that $\xi^* \neq 0$ and $\xi^* \neq 1$.

The flux difference $\delta\mathbf{F}_{i-1/2} = \mathbf{F}(\mathbf{U}_i) - \mathbf{F}(\mathbf{U}_{i-1})$ can obviously be written as

$$\delta\mathbf{F}_{i-1/2} = [\mathbf{F}(\mathbf{U}_i) - \mathbf{F}(\mathbf{U}_R)] + [\mathbf{F}(\mathbf{U}_R) - \mathbf{F}(\mathbf{U}_L)] + [\mathbf{F}(\mathbf{U}_L) - \mathbf{F}(\mathbf{U}_{i-1})] \tag{38}$$

and then transformed using (37) and the Jacobian definition $\mathbf{A} = \partial\mathbf{F}/\partial\mathbf{U}$ into

$$\delta\mathbf{F}_{i-1/2} = \int_{\xi^*}^{1} \mathbf{A}(\xi)\,\mathrm{d}\xi \cdot \frac{\mathbf{U}_i - \mathbf{U}_R}{1-\xi^*} + [\mathbf{F}(\mathbf{U}_R) - \mathbf{F}(\mathbf{U}_L)] + \int_{0}^{\xi^*} \mathbf{A}(\xi)\,\mathrm{d}\xi \cdot \frac{\mathbf{U}_L - \mathbf{U}_{i-1}}{\xi^*}. \tag{39}$$

So far an arbitrary discontinuity has been considered. The integrals in (39) can be subjected to the artificial wind transformation (3) and, thus, converted into the sums of perturbations moving in a certain direction. However, the flux difference across the discontinuity may be associated with a disturbance having a certain direction of propagation (which is crucial for upwinding) only in cases of a physical discontinuity propagating with a speed D_H, at which the Rankine–Hugoniot relations hold:

$$\mathbf{F}(\mathbf{U}_R) - \mathbf{F}(\mathbf{U}_L) = D_H(\mathbf{U}_R - \mathbf{U}_L). \tag{40}$$

That is why only physical discontinuities are considered in all subsequent analyses.

Under such conditions we may apply the artificial wind transformation (3) in the same way as we did in Section 4 to all terms in (39), including the flux difference across the discontinuity:

$$\begin{aligned} \delta\mathbf{F}_{i-1/2} = {} & \int_{\xi^*}^{1} [\mathbf{A}(\xi) - D^L(\xi)\mathbf{E}]\,\mathrm{d}\xi \cdot \frac{\mathbf{U}_i - \mathbf{U}_R}{1-\xi^*} + [\mathbf{F}(\mathbf{U}_R) - \mathbf{F}(\mathbf{U}_L)] - D^C(\mathbf{U}_R - \mathbf{U}_L) \\ & + \int_{0}^{\xi^*} [\mathbf{A}(\xi) - D^R(\xi)\mathbf{E}]\,\mathrm{d}\xi \cdot \frac{\mathbf{U}_L - \mathbf{U}_{i-1}}{\xi^*}. \end{aligned} \tag{41}$$

Here D^C is the artificial wind velocity for the internal discontinuity, changing its propagation speed, which now becomes equal to $D_H - D^C$. The artificial wind velocities $D^L(\xi)$ and $D^R(\xi)$ are defined in (20) and (22).

To keep the equality (39) intact we should require that all added terms result in a zero sum:

$$\int_{\xi^*}^{1} D^L(\xi)\,\mathrm{d}\xi \cdot \frac{\mathbf{U}_i - \mathbf{U}_R}{1-\xi^*} + D^C(\mathbf{U}_R - \mathbf{U}_L) + \int_0^{\xi^*} D^R(\xi)\,\mathrm{d}\xi \cdot \frac{\mathbf{U}_L - \mathbf{U}_{i-1}}{\xi^*} = 0. \quad (42)$$

To be consistent with previous developments without internal discontinuities (Section 4) let us assume, analogously to (26), that

$$d = \int_0^{\xi^*} D^R(\xi)\,\mathrm{d}\xi = -\int_{\xi^*}^{1} D^L(\xi)\,\mathrm{d}\xi. \quad (43)$$

Then we suppose that there is a parameter $\xi^c (0 \le \xi^c \le 1)$ at which

$$\mathbf{U}_{i-1} \cdot (1-\xi^*) + \mathbf{U}_i \cdot \xi^* = \mathbf{U}_L \cdot (1-\xi^c) + \mathbf{U}_R \cdot \xi^c. \quad (44)$$

Substituting (43) and (44) into (42) the following expression for the artificial wind velocity D^C can be easily derived:

$$D^C = \frac{d \cdot (\xi^c - \xi^*)}{\xi^* \cdot (1-\xi^*)}. \quad (45)$$

For $\xi^c = \xi^*$ we have $D^C = 0$.

Delegating the discussion on physical meaning of the above formulas into the next subsection we now construct the upwind flux $\mathbf{F}_{i-1/2}$.

Analogously to Section 4 and according to the artificial wind definitions (20) and (22) the first integral in (41) is the sum of perturbations propagating to the right while the last one is of those propagating to the left. The flux difference $[\mathbf{F}(\mathbf{U}_R) - \mathbf{F}(\mathbf{U}_L)] - D^C(\mathbf{U}_R - \mathbf{U}_L) = (D_H - D^C)(\mathbf{U}_R - \mathbf{U}_L)$ corresponds to a physical discontinuity with the velocity $D_H - D^C$. It moves to the left if the velocity is negative, and to the right if it is positive.

For $D_H - D^C > 0$, taking into account all disturbances going to the left, we have

$$\mathbf{F}_{i-1/2} = \mathbf{F}_{i-1} + \int_0^{\xi^*} [\mathbf{A}(\xi) - D^R(\xi)\mathbf{E}]\,\mathrm{d}\xi \cdot \frac{\mathbf{U}_L - \mathbf{U}_{i-1}}{\xi^*} = \mathbf{F}(\mathbf{U}_L) - \frac{d}{\xi^*}(\mathbf{U}_L - \mathbf{U}_{i-1}). \quad (46)$$

For $D_H - D^C < 0$, taking into account all disturbances going to the right, we arrive at

$$\mathbf{F}_{i-1/2} = \mathbf{F}_i - \int_{\xi^*}^{1} [\mathbf{A}(\xi) - D^L(\xi)\mathbf{E}]\,\mathrm{d}\xi \cdot \frac{\mathbf{U}_i - \mathbf{U}_R}{1-\xi^*} = \mathbf{F}(\mathbf{U}_R) - \frac{d}{1-\xi^*}(\mathbf{U}_i - \mathbf{U}_R). \quad (47)$$

Simple algebraical transformations using (40), (44), and (45) prove that for $D_H = D^C$ the above two expressions are equal and any of them may be used.

Thus, we eventually obtain the flux expression for the differential AW scheme with a physical discontinuity, which should be used in combination with (40), (43), (44), (45),

(20), (22):

$$\mathbf{F}_{i-1/2}=\begin{cases}\mathbf{F}(\mathbf{U}_R)-\frac{d}{1-\xi^*}(\mathbf{U}_i-\mathbf{U}_R) & \text{if } D_H-D^C\le 0,\\ \mathbf{F}(\mathbf{U}_L)-\frac{d}{\xi^*}(\mathbf{U}_L-\mathbf{U}_{i-1}) & \text{if } D_H-D^C\ge 0.\end{cases} \tag{48}$$

Expression (48) can be also rewritten in the form

$$\mathbf{F}_{i-1/2}=\tilde{\mathbf{F}}_{i-1/2}+\begin{cases}\mathbf{F}(\mathbf{U}_R)-D^C\mathbf{U}_R & \text{if } D_H-D^C\le 0,\\ \mathbf{F}(\mathbf{U}_L)-D^C\mathbf{U}_L & \text{if } D_H-D^C\ge 0,\end{cases} \tag{49}$$

where

$$\tilde{\mathbf{F}}_{i-1/2}=\frac{d}{\xi^*(1-\xi^*)}[(1-\xi^*)\mathbf{U}_{i-1}-(1-\xi^c)\mathbf{U}_L]=\frac{d}{\xi^*(1-\xi^*)}[\xi^c\mathbf{U}_R-\xi^*\mathbf{U}_i]. \tag{50}$$

6.3. Physical Interpretation

The differential artifical wind scheme with an internal physical discontinuity may be interpreted as the Godunov scheme with a modified initial distribution of gas dynamic parameters in the same way as was done in Section 5.2 (Fig. 4) for the differential AW scheme itself.

At first, we exactly follow the procedure of Section 5.2. Based on the averaged AW velocities (35) two additional interfaces, at $x_L=x_{i-1/2}-D^R_{i-1/2}\Delta t$ and $x_R=x_{i-1/2}-D^L_{i-1/2}\Delta t$, are introduced. The averaged AW velocities $D^L_{i-1/2}$ and $D^R_{i-1/2}$ are supposed to be "large enough" so that the waves of the exact self-similar solutions of the Riemann problems at the additional interfaces do not reach the face $x_{i-1/2}$ during the time step Δt. The weight coefficient ξ^* and the dissipation coefficient d are given via the averaged velocities by (10) and (13).

We can exclude ξ^* and d from the formulas for the differential AW scheme with an internal discontinuity and get equivalent expressions via the averaged AW velocities. The flux (48) may be written as

$$\mathbf{F}_{i-1/2}=\begin{cases}\mathbf{F}(\mathbf{U}_R)+D^L_{i-1/2}(\mathbf{U}_i-\mathbf{U}_R) & \text{if } D_H-D^C\le 0,\\ \mathbf{F}(\mathbf{U}_L)-D^R_{i-1/2}(\mathbf{U}_L-\mathbf{U}_{i-1}) & \text{if } D_H-D^C\ge 0.\end{cases} \tag{51}$$

We note that the equality (45) becomes

$$D^C=\xi^c\left(D^R_{i-1/2}-D^L_{i-1/2}\right)+D^L_{i-1/2}. \tag{52}$$

The relation (44) results in

$$D^R_{i-1/2}(\mathbf{U}_{i-1}-\mathbf{U}_L)-D^L_{i-1/2}(\mathbf{U}_i-\mathbf{U}_L)=\xi^c\left(D^R_{i-1/2}-D^L_{i-1/2}\right)(\mathbf{U}_R-\mathbf{U}_L). \tag{53}$$

Combining (52) and (53) we have an expression useful for subsequent considerations:

$$D^R_{i-1/2}(\mathbf{U}_{i-1}-\mathbf{U}_L)=D^C(\mathbf{U}_R-\mathbf{U}_L)+D^L_{i-1/2}(\mathbf{U}_i-\mathbf{U}_R). \tag{54}$$

Instead of the constant distribution $\bar{\mathbf{U}}(\xi^*)$ between the faces $x=x_L$ and $x=x_R$ we now introduce a piecewise constant distribution with a physical discontinuity positioned at $x_C=x_{i-1/2}-D^C\Delta t$; i.e., its location is determined by the artificial wind velocity D^C assigned to the discontinuity ($D^L_{i-1/2}\le D^C\le D^R_{i-1/2}$), and having the left and right values

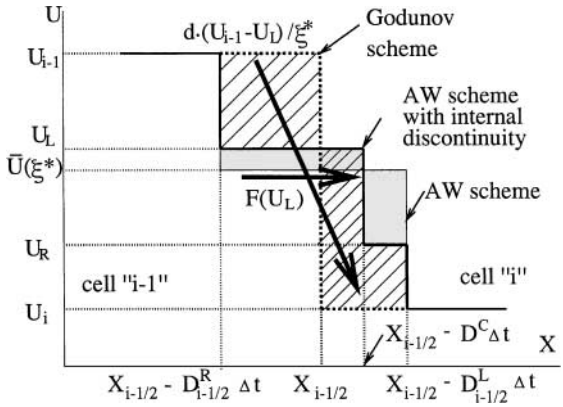

FIG. 5. Schematic of the initial distributions of gas dynamic parameters at a face for the artificial wind (thin solid line), artificial wind with an internal discontinuity (bold solid line), and Godunov (bold dashed line) schemes. Shaded areas are equal; dashed areas on the both sides of the face $x_{i-1/2}$ are equal as well.

equal to $\mathbf{U}_L$ and $\mathbf{U}_R$ (Fig. 5), and the speed of propagation D_H. The internal discontinuity is introduced in such a way that its averaging over the interval $[x_L, x_R]$ results in the same average value $\bar{\mathbf{U}}(\xi^*)$ as the averaging of the original Godunov distribution: this is expressed mathematically by (44) and graphically in Fig. 5—the two shaded areas are equal. It is then obvious that the new weight coefficient ξ^c may be expressed, analogously to (10), as

$$\xi^c = \frac{-D^L_{i-1/2} - (-D^C)}{D^R_{i-1/2} - D^L_{i-1/2}} = \frac{D^C - D^L_{i-1/2}}{D^R_{i-1/2} - D^L_{i-1/2}}, \tag{55}$$

from which the expession (52) for D^C and the inequality $0 \le \xi^c \le 1$ immediately follows. In other words, we replace the original Godunov scheme distribution with a discontinuity at $x_{i-1/2}$ by a three-step distribution with three discontinuities, with the central one being a physical discontinuity. The relation (54) expresses the fact that the dashed areas in Fig. 5 on the left and right sides of the face $x_{i-1/2}$ are equal, too. This confirms that we establish our new distribution in a conservative way.

Let us now show that the application of the Godunov scheme technology to the constructed initial distribution with three discontinuities leads to the flux (51). Indeed, first of all we should consider the exact solutions of the Riemann problems at all three faces, $x = x_L$, $x = x_R$, and $x = x_C$. As in Section 5.2, we are under no obligation to actually calculate the exact solutions at $x = x_L, x = x_R$ since the respective waves do not contribute to the flux $\mathbf{F}_{i-1/2}$.

The exact solution at $x = x_C$ is a physical discontinuity moving with the speed D_H. If $D_H \le D^C$ the discontinuity does not reach the face $x_{i-1/2}$ during the time step (if $D_H = D^C$, it does at the time $t^n + \Delta t$), so the flux $\mathbf{F}_{i-1/2}$ is simply equal to $\mathbf{F}(\mathrm{U}_L)$.

If $D_H \ge D^C$ the discontinuity crosses the face at the time moment $\tilde{t} = t^n + (D^C/D_H)\Delta t$ so that the flux should be calculated as follows:

$$\mathbf{F}_{i-1/2} = \mathbf{F}(\mathbf{U}_L)\frac{D^C}{D_H} + \mathbf{F}(\mathbf{U}_R)\left(1 - \frac{D^C}{D_H}\right) = \mathbf{F}(\mathbf{U}_R) - D^C(\mathbf{U}_R - \mathbf{U}_L). \tag{56}$$

The second equality comes from the Rankine–Hugonoit relations (40).

It should not be forgotten that, as in Section 5.2, the modified initial distribution leads to the modified cell average at the time level n:

$$\frac{1}{\Delta x}\int_{x_{i-1/2}}^{x_{i+1/2}} \mathbf{U}(x, t_n)\,\mathrm{d}x = \mathbf{U}_i^n - \frac{\Delta t}{\Delta x}\left[-D^C(\mathbf{U}_R - \mathbf{U}_L) - D^L_{i-1/2}(\mathbf{U}_i - \mathbf{U}_R)\right]$$

$$= \mathbf{U}_i^n - \frac{\Delta t}{\Delta x} D^R_{i-1/2}(\mathbf{U}_L - \mathbf{U}_{i-1}). \tag{57}$$

The second equality comes from (54). To fit the conservative formulation (31) we again interpret the second term in the above equation as an additional flux across the face and include it in $\mathbf{F}_{i-1/2}$.

Summarizing all contributions we have for $D_H \le D^C$ (using the second equality in (57))

$$\mathbf{F}_{i-1/2} = \mathbf{F}(\mathbf{U}_L) - D^R_{i-1/2}(\mathbf{U}_L - \mathbf{U}_{i-1}), \tag{58}$$

which fully corresponds to (51). For $D_H \ge D^C$ we obtain (combining (56) and the first equality in (57))

$$\mathbf{F}_{i-1/2} = \mathbf{F}(\mathbf{U}_R) - D^C(\mathbf{U}_R - \mathbf{U}_L) + D^C(\mathbf{U}_R - \mathbf{U}_L) + D^L_{i-1/2}(\mathbf{U}_i - \mathbf{U}_R)$$

$$= \mathbf{F}(\mathbf{U}_R) + D^L_{i-1/2}(\mathbf{U}_i - \mathbf{U}_R), \tag{59}$$

again in full agreement with (51).

It is worth noting that the AW velocity D^C and the weight coefficient ξ^c are interrelated via (45) and either may be used to specify the location of the internal discontinuity within the interval $[x_L, x_R]$.

The flux $\tilde{\mathbf{F}}_{i-1/2}$ in (49) and (50) represents the relationship between the amount of a conserved variable within the control volume $[x_L, x_R]$ to the left (or right) of the face $x_{i-1/2}$ before the introduction of an internal discontinuity and that to the left (or right) of the internal discontinuity (x_C) after its introduction (let us note that Eq. (44) (and (50)) may be viewed as a conservation law for the control volume $[x_L, x_R]$).

6.4. The Case of a Contact Discontinuity

To use the differential artificial wind scheme with an internal physical discontinuity in practice, we should specify the type of discontinuity and define the gas dynamic parameters on both sides ($\mathbf{U}_L$, $\mathbf{U}_R$), its velocity D_H, and its initial location (which is defined by either the artificial wind velocity D^C or the weight coefficient ξ^c).

Since we are especially concerned with the resolution of contact discontinuities, let us consider the introduction of a contact discontinuity. Velocity and pressure are continuous across a contact discontinuity, so that we have

$$u_L = u_R = u_C, \tag{60}$$

$$p_L = p_R = p_C, \tag{61}$$

where u_C and p_C are newly introduced notations for the velocity and pressure at the contact discontinuity, respectively. The left and right density values, ρ_L and ρ_R, are generally not equal at the contact discontinuity. Thus, for the artificial wind scheme with a contact discontinuity we should determine the following five parameters: ρ_L, ρ_R, u_C, p_C, and ξ^c.

The Rankine–Hugoniot relations (40) for the contact discontinuity are satisfied under (60) and (61). Thus, the only relation we should satisfy while determining parameters of the contact discontinuity is given by (44).

Let us consider a particular vector of conserved variables $\mathbf{U} = (\rho, \rho u, \rho E)$ (corresponding to the Euler equations) and write out (44) separately for each component of the vector. The specific full energy E is given by $\rho E = \rho e + \rho u^2/2$, where $e = e(p, \rho)$ is the specific internal energy. Taking into account (60) and (61) we have

$$\rho_{i-1} \cdot (1 - \xi^*) + \rho_i \cdot \xi^* = \rho_L \cdot (1 - \xi^c) + \rho_R \cdot \xi^c, \tag{62a}$$

$$\rho_{i-1} u_{i-1} \cdot (1 - \xi^*) + \rho_i u_i \cdot \xi^* = [\rho_L \cdot (1 - \xi^c) + \rho_R \cdot \xi^c] u_C, \tag{62b}$$

$$\begin{aligned}(\rho e)_{i-1} \cdot (1 - \xi^*) + (\rho e)_i \cdot \xi^* + \rho_{i-1} \frac{u_{i-1}^2}{2} \cdot (1 - \xi^*) + \rho_i \frac{u_i^2}{2} \cdot \xi^* \\ = (\rho e)_L \cdot (1 - \xi^c) + (\rho e)_R \cdot \xi^c + [\rho_L \cdot (1 - \xi^c) + \rho_R \cdot \xi^c] \frac{u_C^2}{2}.\end{aligned} \tag{62c}$$

Substituting (62a) into (62b) we have for u_C

$$u_C = \frac{\rho_{i-1} u_{i-1} \cdot (1 - \xi^*) + \rho_i u_i \cdot \xi^*}{\rho_{i-1} \cdot (1 - \xi^*) + \rho_i \cdot \xi^*}. \tag{63}$$

Simple transformations allow us to write the remaining two equations as

$$\rho_{i-1} \cdot (1 - \xi^*) + \rho_i \cdot \xi^* = \rho_L \cdot (1 - \xi^c) + \rho_R \cdot \xi^c, \tag{64a}$$

$$\begin{aligned}(\rho e)_{i-1} \cdot (1 - \xi^*) + (\rho e)_i \cdot \xi^* + \delta Q_k \\ = \rho_L \cdot e(p_C, \rho_L) \cdot (1 - \xi^c) + \rho_R \cdot e(p_C, \rho_R) \cdot \xi^c,\end{aligned} \tag{64b}$$

where the difference in kinetic energy δQ_k is given by

$$\delta Q_k = \frac{1}{2} \cdot \frac{\rho_{i-1} \rho_i (1 - \xi^*) \xi^* (u_i - u_{i-1})^2}{\rho_{i-1} \cdot (1 - \xi^*) + \rho_i \cdot \xi^*} \geq 0. \tag{65}$$

Equations (64a) and (64b) contain four unknowns: ρ_L, ρ_R, p_C, and ξ^c. Thus, the solution of the system is not unique. The fact that we face multiple choices may also be illustrated, for instance, by the observation that the assumption of $\rho_L = \rho_R$, i.e., of the contact discontinuity of zero intensity, is a valid choice. In such a case the flux expressions (48) become identical and equal to the flux of the differential AW scheme (25) regardless of the values of D_C and ξ^c (this corresponds to the obvious fact that the contact discontinuity of zero intensity may be placed anywhere).

Thus, some additional requirements should be involved to complete the introduction of a contact discontinuity. We propose here the following way which may not be the only possible one. The contact discontinuity should be set up consistently with density distribution, i.e.,

$$\rho_{i-1} \cdot (1 - \xi^*) = \rho_L \cdot (1 - \xi^c) \tag{66a}$$

or

$$\rho_L = \rho_{i-1} \cdot \frac{1 - \xi^*}{1 - \xi^c}, \tag{66b}$$

from where it immediately follows, taking into account (64a), that

$$\rho_i \cdot \xi^* = \rho_R \cdot \xi^c \tag{67a}$$

or

$$\rho_R = \rho_i \cdot \frac{\xi^*}{\xi^c}. \tag{67b}$$

This means that the mass to the left and to the right of the face $x_{i-1/2}$ is equal to the respective value to the left and to the right of the introduced contact discontinuity. In other words, the mass flux in (50) equals 0. Using (66a) and (67a) we may find p_C from (64b).

The last parameter to be determined is the weight coefficient ξ^c defining the location of the contact discontinuity with $[x_L, x_R]$. The condition for ξ^c may be derived, for instance, from the requirement that the scheme should possess the nondecreasing total entropy property; i.e., the inequalities

$$\begin{cases} \rho_{i-1} s_{i-1} \cdot (1 - \xi^*) \le \rho_L \cdot s(p_C, \rho_L) \cdot (1 - \xi^c) \\ \rho_i s_i \cdot \xi^* \le \rho_R \cdot s(p_C, \rho_R) \cdot \xi^c \end{cases} \tag{68}$$

or, which is the same in view of (66a) and (67a),

$$\begin{cases} s_{i-1} \le s(p_C, \rho_L) \\ s_i \le s(p_C, \rho_R), \end{cases} \tag{69}$$

where $s = s(p, \rho)$ is the specific entropy, should be satisfied. In other words, we transform the original Godunov scheme initial distribution into that for the differential AW scheme with the contact discontinuity (see Fig. 5) in an isentropic way. Since after establishing the modified initial distribution we strictly follow the Godunov scheme procedure, the whole scheme will not decrease entropy under (69) (see the end of Section 5.2). The full averaging of density ($\rho_L = \rho_R$) used in the differential artificial wind scheme satisfies (69) and, moreover, results in the maximum possible production of entropy.

The inequalities (69) in fact mean that we have a range of ξ^c values not decreasing entropy:

$$(\xi^c)_L \le \xi^c \le (\xi^c)_R. \tag{70}$$

The value $(\xi^c)_{\max}$ corresponding to the maximum entropy production (i.e., to the maximum of the function $\Delta s = \rho_{i-1}(1 - \xi^*)(s_L - s_{i-1}) + \rho_i \xi^* (s_R - s_i)$ at which $\rho_L = \rho_R$) generally may or may not belong to the interval (70). To assign a specific value ξ^c from (70) it seems, at first glance, logical to minimize the entropy production (while (69) holds!). However, it is easy to see that this would lead to a discontinuous variation of ξ^c, i.e., nonphysical "jumps" of the contact discontinuity. Numerical trials show that in practice this leads to a very nonrobust scheme. We propose here the opposite, maximizing the entropy production under the conditions (69). If $(\Delta s)''_{\xi^c} < 0$ the expression

$$\xi^c = \min\{\max\{(\xi^c)_L, (\xi^c)_{\max}\}, (\xi^c)_R\}, \tag{71}$$

providing a smooth variation of ξ^c, can be suggested.

So far our considerations are very general. To proceed further toward practical formulas and computations, we should define the equation-of-state $e = e(p, \rho)$. Let us consider here the case of a perfect gas with a constant specific heat ratio γ and a gas constant R for which $\rho e = p/(\gamma - 1)$, $c = \sqrt{\gamma(p/\rho)}$, $s = [R/(\gamma - 1)] \ln(p/\rho^\gamma) + \text{const}$.

The full set of formulas for the perfect gas case is listed below:

$$\mathbf{F}_{i-1/2} = \begin{cases} \mathbf{F}(\mathbf{U}_R) - \frac{d}{1-\xi^*}(\mathbf{U}_i - \mathbf{U}_R) & \text{if } u_C - D^C \le 0, \\ \mathbf{F}(\mathbf{U}_L) - \frac{d}{\xi^*}(\mathbf{U}_L - \mathbf{U}_{i-1}) & \text{if } u_C - D^C \ge 0; \end{cases} \tag{72a}$$

$$D^C = \frac{d \cdot (\xi^c - \xi^*)}{\xi^* \cdot (1 - \xi^*)}; \tag{72b}$$

$$u_C = u_L = u_R = \frac{\rho_{i-1} u_{i-1} \cdot (1 - \xi^*) + \rho_i u_i \cdot \xi^*}{\rho_{i-1} \cdot (1 - \xi^*) + \rho_i \cdot \xi^*}; \tag{72c}$$

$$p_C = p_L = p_R = p_{i-1} \cdot (1 - \xi^*) + p_i \cdot \xi^* + \delta Q_k(\gamma - 1); \tag{72d}$$

$$\delta Q_k = \frac{1}{2} \cdot \frac{\rho_{i-1}\rho_i(1 - \xi^*)\xi^*(u_i - u_{i-1})^2}{\rho_{i-1} \cdot (1 - \xi^*) + \rho_i \cdot \xi^*}; \tag{72e}$$

$$\rho_L = \rho_{i-1} \cdot \frac{1 - \xi^*}{1 - \xi^c}, \quad \rho_R = \rho_i \cdot \frac{\xi^*}{\xi^c}; \tag{72f}$$

$$\xi^c = \min\{\max\{(\xi^c)_L, (\xi^c)_{\max}\}, (\xi^c)_R\}, \quad (\xi^c)_L = \xi^* \left(\frac{p_i}{p_C}\right)^{1/\gamma}; \tag{72g}$$

$$(\xi^c)_R = 1 - (1 - \xi^*)\left(\frac{p_{i-1}}{p_C}\right)^{1/\gamma}, \quad (\xi^c)_{\max} = \frac{\rho_i \xi^*}{\rho_{i-1} \cdot (1 - \xi^*) + \rho_i \cdot \xi^*}; \tag{72h}$$

$$d = \int_0^{\xi^*} D^R(\xi)\, d\xi = -\int_{\xi^*}^1 D^L(\xi)\, d\xi; \tag{72i}$$

$$D^R(\xi) = \max\{0, u(\xi) + c(\xi)\}, \quad D^L(\xi) = \min\{0, u(\xi) - c(\xi)\}. \tag{72j}$$

The value of ξ^* is to be found using the same iteration procedure, (27a), (27b), (27c), (28) (the considerations of Section 4 that for the majority of nodes the iterations are not needed while for the rest of them only one iteration should be performed are valid here as well). To compute $u(\xi^{*(k)}) \pm \sqrt{\gamma p(\xi^{*(k)})/\rho(\xi^{*(k)})}$ the formulas (72g), (72c), (72d), (72f) are used. Since $\delta Q_k \sim (\Delta x)^2$ for smooth solutions we may neglect it, although this does not lead to a significant gain in efficiency since almost all quantities in (72e) should be computed anyway.

The test results in Figs. 6a–6e convincingly show that the incorporation of an internal contact discontinuity into the differential AW scheme improves the numerical solution. In fact, it is basically the same as that produced by the Godunov scheme.

It is worth noting that for linear approximation the differential AW scheme with contact discontinuity is identical to the Godunov scheme.

In many practical problems, the respective conservation laws include, in addition to or instead of the discontinuity equation, equations of the type

$$\frac{\partial(\rho\alpha)}{\partial t} + \frac{\partial(\rho u \alpha)}{\partial x} = 0, \tag{73}$$

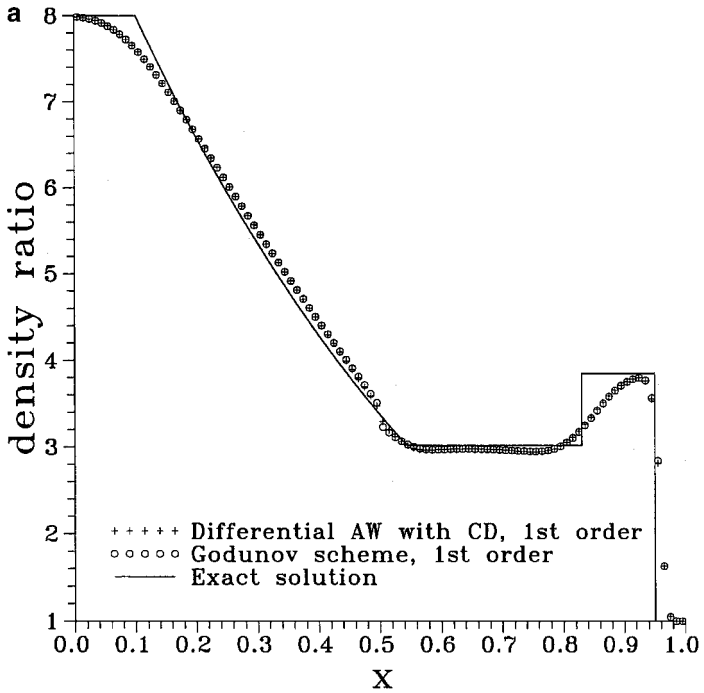

FIG. 6a. Comparison of the first-order differential AW with contact discontinuity and Godunov schemes using the "480 : 1" test problem ($p_2/p_1 = 480$, $\rho_2/\rho_1 = 8$, $u_2 = u_1 = 0$, $\gamma = 5/3$, 100 grid cells, CFL = 0.8).

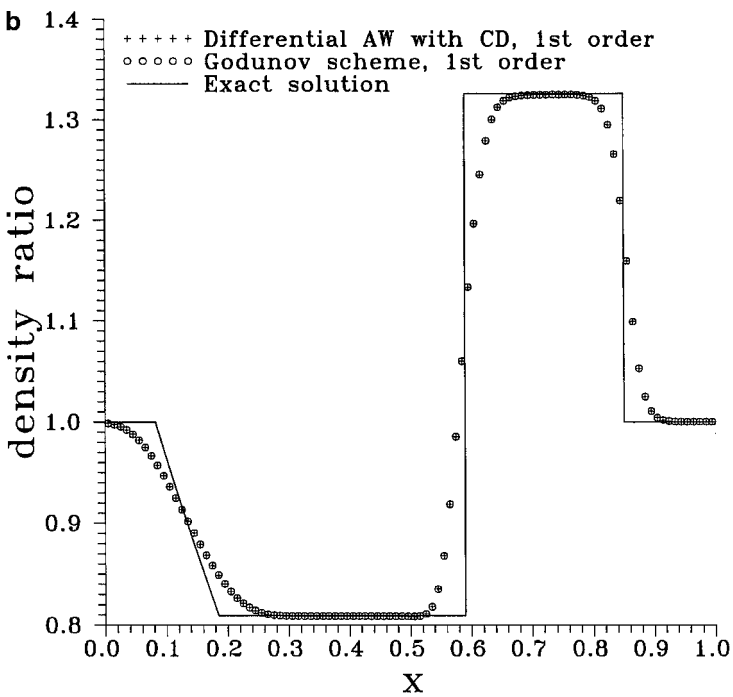

FIG. 6b. Comparison of the first-order differential AW with contact discontinuity and Godunov schemes using the "2 : 1" test problem ($p_2/p_1 = 2$, $\rho_2/\rho_1 = 1$, $u_2 = u_1 = 0$, $\gamma = 1.4$, 100 grid cells, CFL = 0.8).

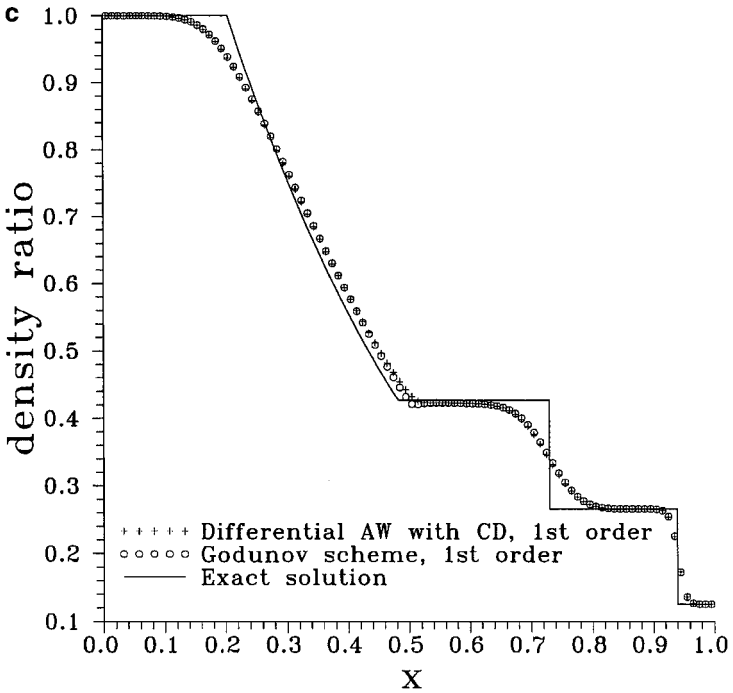

FIG. 6c. Comparison of the first-order differential AW with contact discontinuity and Godunov schemes using the Sod test problem ($p_2 = 1$, $p_1 = 0.1$, $\rho_2 = 1$, $\rho_1 = 0.125$, $u_2 = u_1 = 0$, $\gamma = 1.4$, 100 grid cells, CFL = 0.8).

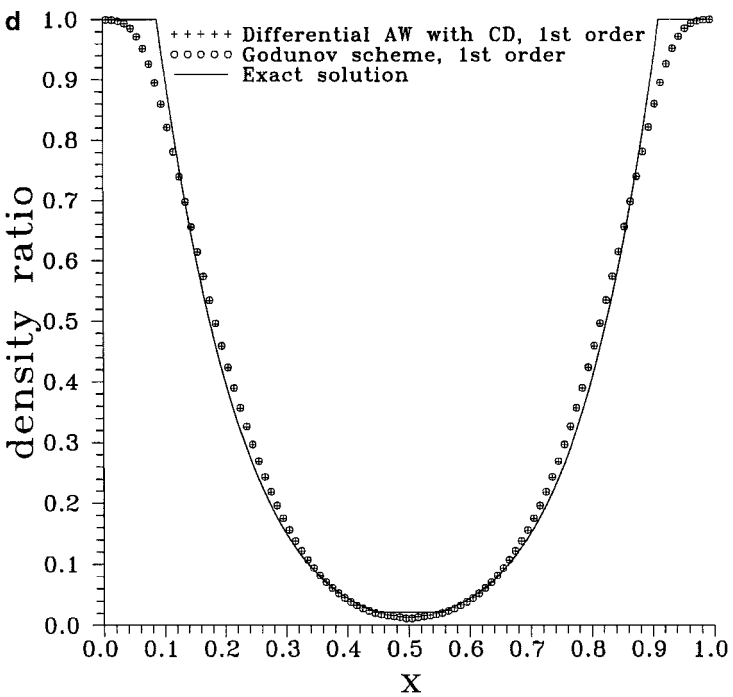

FIG. 6d. Comparison of the first-order differential AW with contact discontinuity and Godunov schemes using the "vacuum" test problem ($p_2 = p_1 = 0.4$, $\rho_2 = \rho_1 = 1$, $u_2 = -2$, $u_1 = 2$, $\gamma = 1.4$, 100 grid cells, CFL = 0.8).

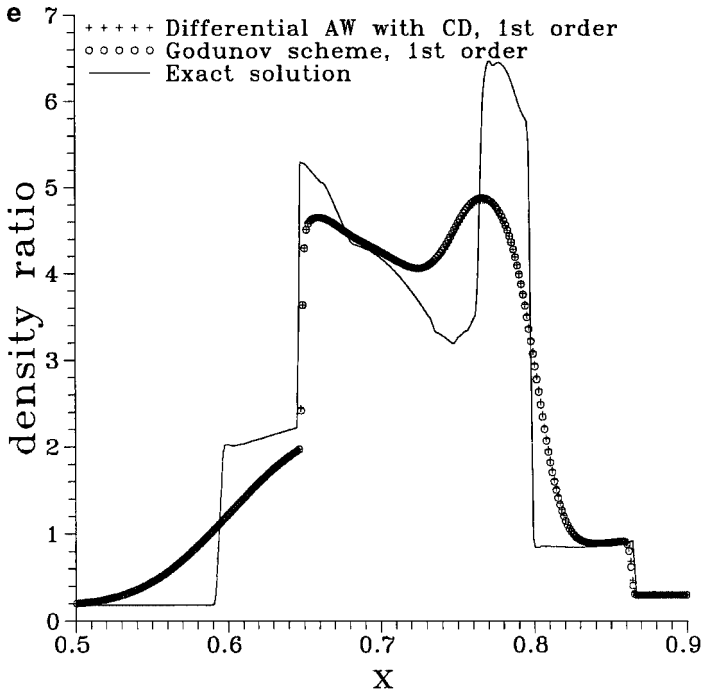

FIG. 6e. Comparison of the first-order differential AW with contact discontinuity and Godunov schemes using the Woodward and Colella test problem ($\gamma = 1.4$, 800 grid cells, CFL = 0.8).

where α is some transported quantity (for instance the mass fraction of a species, etc.). When treating such equations by the differential AW scheme with an internal contact discontinuity, we can assume, regardless of how many of them we have, that

$$\alpha_{i-1} = \alpha_L, \tag{74a}$$

$$\alpha_i = \alpha_R \tag{74b}$$

This is possible because under (66a) and (67a) the choice (74a), (74b) ensures that the vector equation (44) holds for all Eqs. (73) (and the respective components of $\tilde{\mathbf{F}}_{i-1/2}$ in (50) corresponding to the transport of α equal 0). It is worth noting that the same treatment may be prescribed for velocity components tangential to a control volume face when considering multidimensional problems.

7. SECOND-ORDER AND MULTIDIMENSIONAL EXTENSIONS

In the present paper we do not venture into considerations of an optimal and/or inherent way to extend the artificial wind schemes to the second order of accuracy and two or three spatial dimensions. This will be explored elsewhere. Here we just demonstrate that the application of conventional, widely used approaches leads to quite good results.

Out of numerous available choices (see [5, 12]) of higher order extensions for upwind schemes we employ here a MUSCL predictor–corrector approach generally attributed to Hancock (see [5]), although in Russian literature it is usually associated with the Rodionov scheme ([13]). When used in combination with the exact Riemann solver it may be considered a typical second-order extension of the Godunov scheme. The technique has some

attractive features, being accurate and rather robust, with a simple predictor step without any Riemann solvers, which contributes to efficiency, and easily applicable to any kind of grid, structured or unstructured alike. In fact, we have used it quite extensively in various applications during the last decade (see [14]).

At the first stage, we find the limited gradients of the primitive variables $\mathbf{V} = (\rho, u, p)$ at each grid node,

$$\overline{\Delta \mathbf{V}_i} = L\big(\mathbf{V}^n_{i+1} - \mathbf{V}^n_i, \mathbf{V}^n_i - \mathbf{V}^n_{i-1}\big), \tag{75}$$

where $L(a, b)$ is a flux limiter function eliminating spurious oscillations near discontinuties. The predictor step is

$$\tilde{\mathbf{U}}_i = \mathbf{U}^n_i - \frac{\Delta t}{\Delta x}\big(\mathbf{F}\big(\mathbf{V}^l_{i+1/2}\big) - \mathbf{F}\big(\mathbf{V}^r_{i-1/2}\big)\big), \tag{76}$$

where

$$\mathbf{V}^l_{i+1/2} = \mathbf{V}^n_i + 0.5\overline{\Delta \mathbf{V}}_i, \quad \mathbf{V}^r_{i-1/2} = \mathbf{V}^n_i - 0.5\overline{\Delta \mathbf{V}}_i. \tag{77}$$

The corrector step is given by

$$\mathbf{U}^{n+1}_i = \mathbf{U}^n_i - \frac{\Delta t}{\Delta x}\big(\mathbf{F}\big(\tilde{\mathbf{V}}^l_{i+1/2}, \tilde{\mathbf{V}}^r_{i+1/2}\big) - \mathbf{F}\big(\tilde{\mathbf{V}}^l_{i-1/2}, \tilde{\mathbf{V}}^r_{i-1/2}\big)\big), \tag{78}$$

where

$$\tilde{\mathbf{V}}^r_{i-1/2} = 0.5\big(\mathbf{V}^n_i + \tilde{\mathbf{V}}_i - \overline{\Delta \mathbf{V}}_i\big), \tag{79}$$

$$\tilde{\mathbf{V}}^l_{i-1/2} = 0.5\big(\mathbf{V}^n_{i-1} + \tilde{\mathbf{V}}_{i-1} + \overline{\Delta \mathbf{V}}_{i-1}\big). \tag{80}$$

Although the predictor step is nonconservative, its results are used in a way that ensures the conservative property of the scheme as a whole. The method provides second-order accuracy in space and time for smooth solutions.

The corrector fluxes should be evaluated via a first-order upwind scheme. In the results presented below either the exact Riemann solver is used (thus resulting in the second-order extension of the Godunov scheme) or the differential artificial wind fluxes are used (which leads to the second-order version of the schemes proposed in this paper).

The second-order results of the differential AW schemes and the Godunov scheme are shown in Figs. 7a–7e. One can see that in some regions the Godunov scheme is slightly better; in others the AW scheme is. These minor differences are strongly influenced by the flux limiters and the type of predictor step. Overall, the same good degree of correspondence as the first-order results have with the Godunov scheme itself is exhibited with the second-order extension of the Godunov scheme.

The kink near the sonic point (test 480 : 1) is not observable anymore for either scheme. The 2 : 1 and Woodward and Collela tests show that the incorporation of a contact discontinuity into the differential AW scheme helps to improve numerical solution, although the difference is not so dramatic as in the first-order case. Generally, in all cases one can see that the differential AW schemes provide results of the same accuracy as those of the Godunov scheme while being simpler and, thus, more efficient. They are about 20–60%

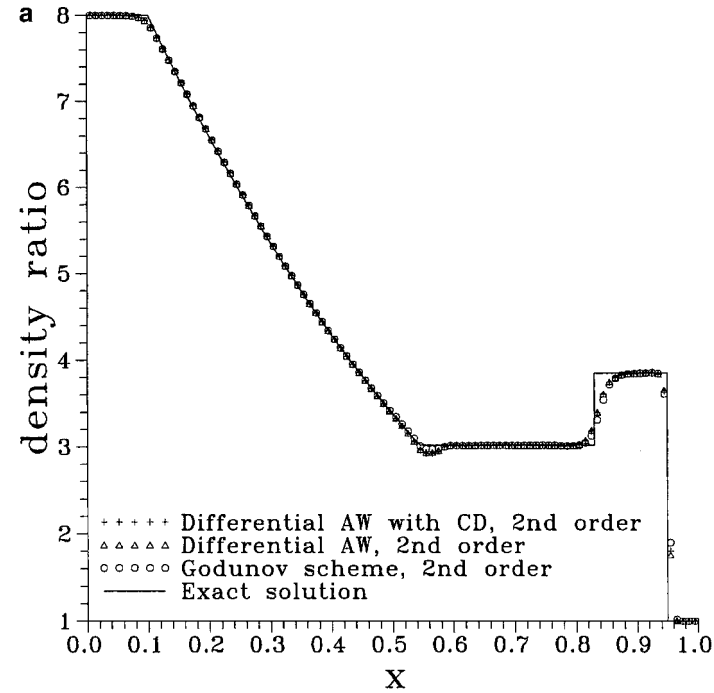

FIG. 7a. Comparison of the second-order differential AW, differential AW with contact discontinuity, and Godunov schemes using the "480 : 1" test problem ($p_2/p_1 = 480$, $\rho_2/\rho_1 = 8$, $u_2 = u_1 = 0$, $\gamma = 5/3$, 100 grid cells, CFL = 0.8).

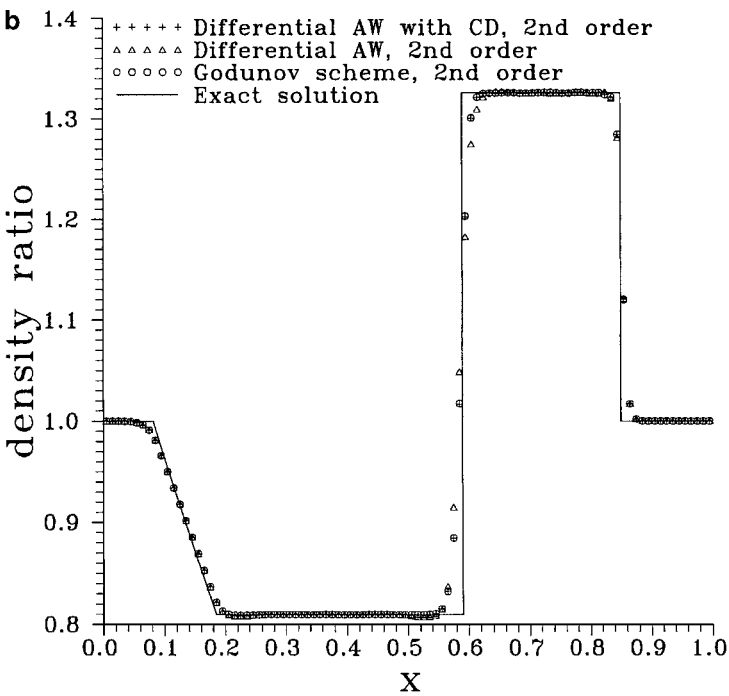

FIG. 7b. Comparison of the second-order differential AW, differential AW with contact discontinuity, and Godunov schemes using the "2 : 1" test problem ($p_2/p_1 = 2$, $\rho_2/\rho_1 = 1$, $u_2 = u_1 = 0$, $\gamma = 1.4$, 100 grid cells, CFL = 0.8).

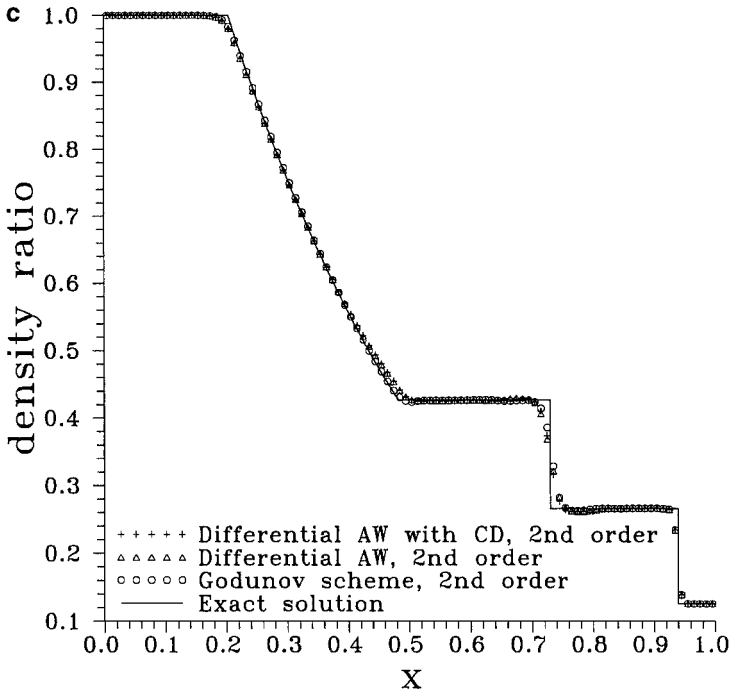

FIG. 7c. Comparison of the second-order differential AW, differential AW with contact discontinuity, and Godunov schemes using the Sod test problem ($p_2 = 1$, $p_1 = 0.1$, $\rho_2 = 1$, $\rho_1 = 0.125$, $u_2 = u_1 = 0$, $\gamma = 1.4$, 100 grid cells, CFL = 0.8).

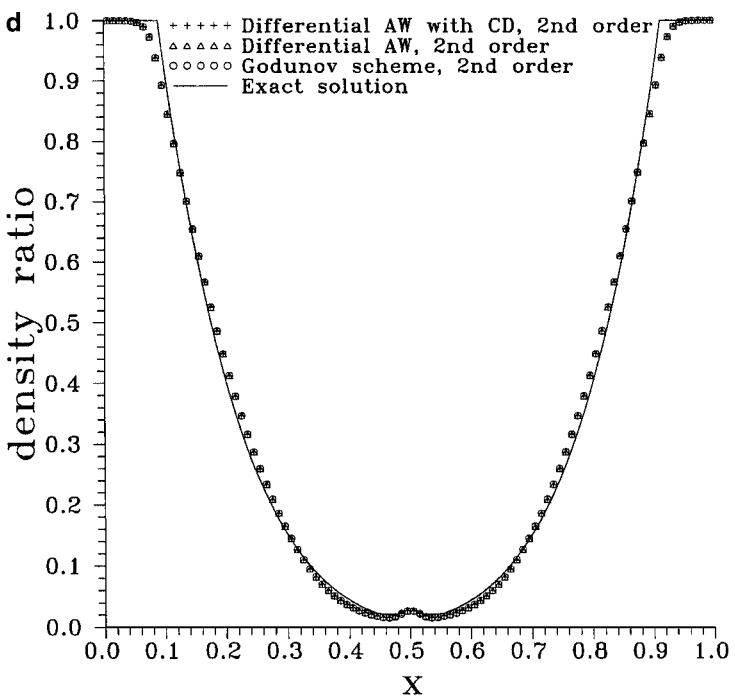

FIG. 7d. Comparison of the second-order differential AW, differential, AW with contact discontinuity, and Godunov schemes using the "vacuum" test problem ($p_2 = p_1 = 0.4$, $\rho_2 = \rho_1 = 1$, $u_2 = -2$, $u_1 = 2$, $\gamma = 1.4$, 100 grid cells, CFL = 0.8).

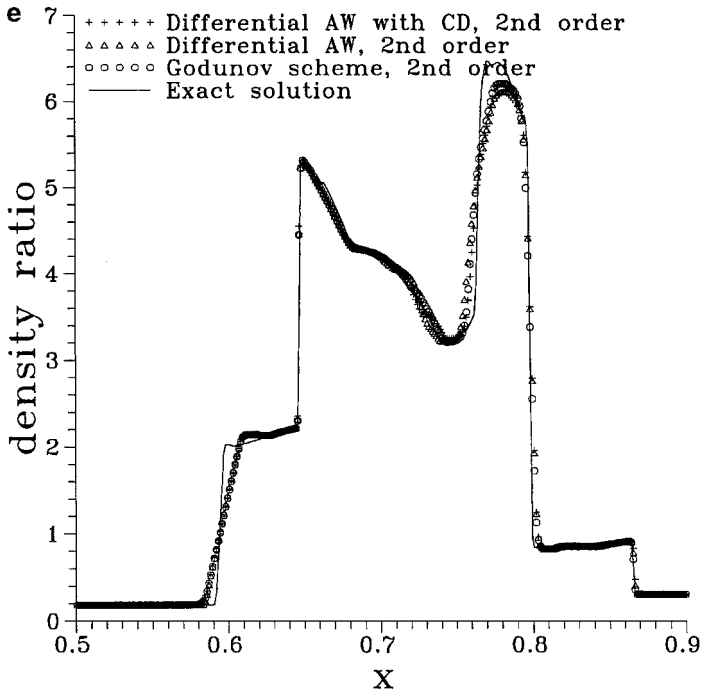

FIG. 7e. Comparison of the second-order differential AW, differential AW with contact discontinuity, and Godunov schemes using the Woodward and Colella test problem ($\gamma = 1.4$, 800 grid cells, CFL = 0.8).

faster depending upon the problem under consideration, the version of the AW schemes used, and specifics of their implementation (number of iterations, etc.).

To perform a 2D test the AW schemes were incorporated into the locally adaptive unstructured Euler code by Voinovich [15]. The finite-volume code is based on a triangular unstructured grid with control volumes being constructed around each node. The respective formulas may be found in [14, 16] and very closely resemble (76), (78), with the summation of fluxes for all faces (in 1D cases we have just two faces). In the original code an exact Riemann solver is used to compute fluxes at each face from the "left" and "right" values. It was replaced by a subroutine embodying the AW schemes with the same input and output variables.

Shock wave diffraction over 90° corner is considered a representative 2D test problem. Once it was used as a benchmark problem at the International Symposium on Shock Waves (see [17]). A fixed (non-solution-adaptive) uniform unstructured triangular grid of moderate spacing (34,850 nodes in total) was used to reveal clearly the differences between the schemes under examination, if any.

The results for the shock Mach number 2.0 ($\gamma = 1.4$) are shown in Fig. 8. The values of density contour lines are exactly the same for each subfigure (starting from 0.01 with 0.08 step). At first glance, the images are nearly identical. However, closer inspection reveals some differences near the wall downstream from the corner, at the tangential discontinuity shed from the corner and rolling up into a vortex, at the contact discontinuity behind the diffracted shock. The local AW scheme (Fig. 8a) provides most diffusive results, which are slightly better for the differential AW approach (Fig. 8b). The inclusion of contact

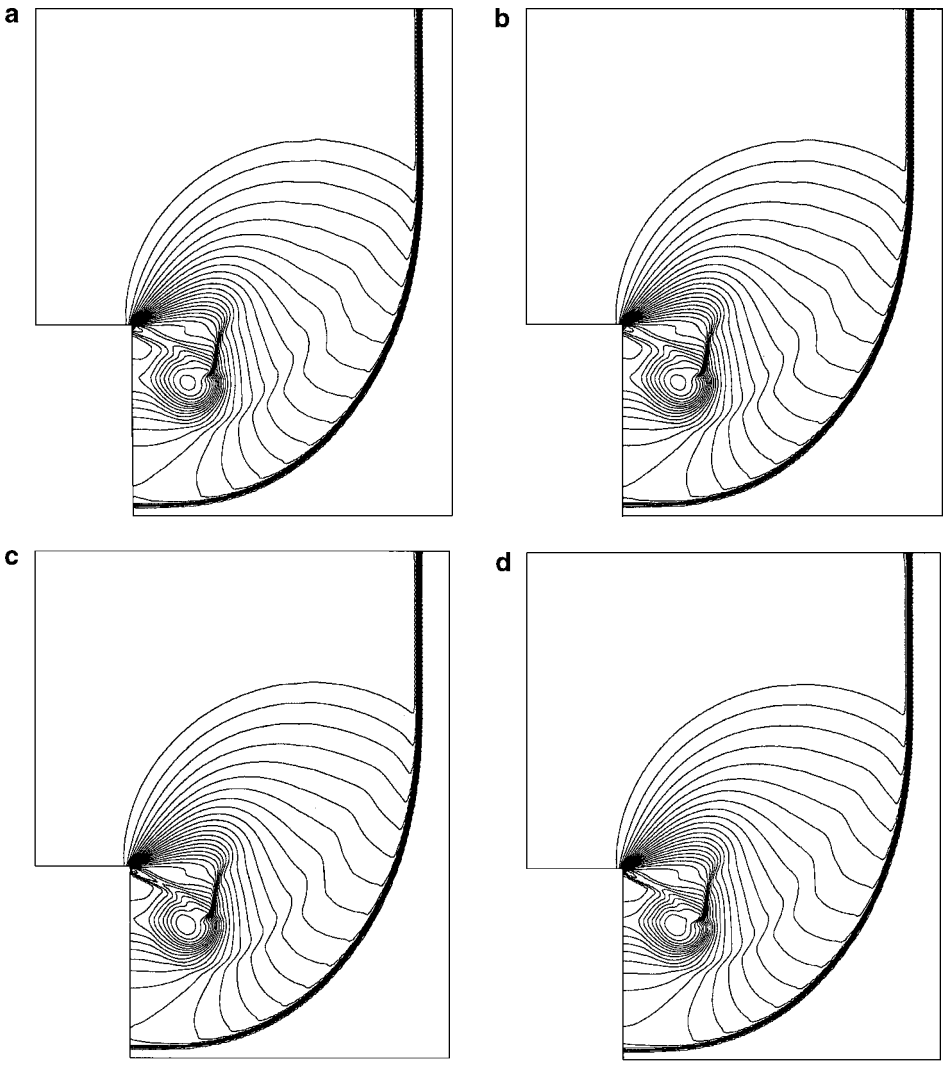

FIG. 8. Comparison of the second-order local AW (a), differential AW (b), differential AW with contact discontinuity (c), and Godunov (d) schemes for shock wave diffraction ($M_s = 2.0$, $\gamma = 1.4$) over a 90° corner (34,850 grid nodes, CFL = 0.7).

discontinuity into the differential AW algorithm (Fig. 8c) sharply improves all features related to contact and tangential discontinuities. The result becomes identical, or perhaps even superior in some places, to the Godunov scheme (Fig. 8c). Similar to the 1D case, the AW schemes are faster than the Godunov one by 20–60%.

8. BRIEF REVIEW OF APPLICATIONS

The main driving force behind the present work was our desire to develop a numerical technique which could be easily, with or without minor generalization efforts, applied to a variety of hydrodynamic problems involving quite different and complex physicomathematical

models, which we were facing. That is why the artificial wind development has been progressing alongside its application to various phenomena prior to the publication of the present account on the general AW methodology. In the present section we very briefly outline what has been done so far in this direction, referring to other papers for specific details. An illustrated review of AW application may also be found in [18].

First, we mention here the studies of shock wave propagation in water assuming that the Tait equation of state is valid and employing the locally adaptive unstructured 2D and 3D codes [14]. In fact, almost the same formulas as those for perfect gases can be used in this case. The only difference is that the expressions for the internal energy and the speed of sound should be slightly modified as follows from the Tait equation. Two problems were analyzed. The first one is the long-distance propagation of a shock wave produced in the ocean by the impact of a celestial body ([19]), involving shock wave interaction with the ocean free surface and deep ocean sound channel. The second problem is the interaction of underwater shock waves induced by an explosion of mild detonating fuses ([18]): two submerged segments of mild detonation fuse are attached to each other at a certain angle and ignited simultaneously at the opposite ends; the detonation wave propagates along the explosive wires and induces axisymmetrical underwater shock waves which, upon completion of the detonation, interact with each other.

Another area to which the artificial wind schemes can be successively applied is magnetohydrodynamics. A spherically imploding plasma motion in a reversed spherical plasma corona created by a powerful laser is analyzed in [20] as a possible way to generate a strong magnetic field. Another example of magnetohydrodynamic applications is an interesting case of magnetic reconnection (incomplete reconnection and complete reconnection), with sophisticated changes in the magnetic field topology taking place during the evolution of two rotating plasma filaments carrying electric current ([21]). In [22] the artificial wind scheme is applied to the simulation of the dissipation of surface Alfvén waves and plasma flows moving upward along the small-scale magnetic flux tubes that emerge from and return to the photosphere with a typical height of about 2000 km within the chromosphere.

The artificial wind schemes for relativistic hydrodymanics may be developed considering the Lorentz invariance instead of the Galilean one. Although the invariant transformation is quite different, the resulting technique after applying the idea of artificial wind is very close to that for the nonrelativistic case. The scheme and some results related to the propagation of a relativistic jet through the interstellar medium and the relativistic case of the Richtmyer–Meshkov instability are given in [8, 23].

It turns out that for magnetohydrodynamics and relativistic hydrodynamics the artificial wind schemes result in numerial solutions of quite reasonable quality, being at the same time more than one order of magnitude faster than traditional techniques (see the papers cited above).

Preliminary analysis shows that the artificial wind schemes may be applied to some electrohydrodynamics models describing the motion of electrically charged fluids to integrate both the hydrodynamic and Maxwell equations. Another prospective application area is the simulation of elastic waves in solids and liquids.

9. CONCLUSIONS

In the present paper we have elaborated on a new general *framework* to construct upwind shock-capture schemes for hyperbolic systems of conservation laws based on the newly

introduced artificial wind concept. The framework applicable to a wide range of physical problems should be viewed as an alternative to other well-known general approaches, such as the Godunov approach, approximate Riemann solvers, and flux-splitting techniques. Naturally, it allows us to derive some already existing schemes or their modifications as well as to develop new ones. It is also possible to apply the AW approach for simplification of already known upwind schemes.

The new schemes possess the following important properties:

- Their final expressions are simple and, what is of extraordinary importance, retain basically the same simple form for a broad range of hydrodynamic problems not requiring cumbersome generalizations.
- They are at least of the same good accuracy as that provided by other widely used upwind schemes.
- The simplicity leads to computational efficiency. Although the gains in computational time for the Euler equation/perfect gas model are not dramatic (about two to three times faster at best), they become very impressive for more complex hydrodynamical systems, such as magnetohydrodynamics, relativistic hydrodynamics, and so forth (up to more than one order of magnitude in some cases, as our experience with practical applications suggests).

It should be emphasized here that the differential AW scheme does not belong to approximate Riemann solvers and thus differs fundamentally from the HLL/HLLC approach. For a nonlinear hyperbolic equation with a convex flux it is identical to the Godunov scheme, while for the hydrodynamic set of equations it represents a modification of the Godunov scheme, with a different initial distribution of parameters based on the *exact* solution of the Riemann problem.

The generality of the artificial wind approach stems from the fact that it is solely based upon the fundamental spatial–temporal transformational properties of hyperbolic systems. No other assumptions are made except the requirement of entropy nondecreasing for the differential AW scheme with contact discontinuity. In the case of nonrelativistic hydrodynamics these transformational properties are the consequence of the Galilean invariance. Upwinding task becomes easily and efficiently solvable using the AW transformation. A specific flux function and equation of state are needed in an explicit form only at the very end, when deriving final formulas to be included in computer codes.

It should be noted that the ways to apply the artificial wind concept for constructing upwind schemes proposed in the present paper may not exhaust all possibilities. Other options implementing the general idea of artifical wind may be found later on. There are also many alternatives mentioned in the derivations of the present paper which need to be explored.

APPENDIX A: DESCRIPTION OF TEST PROBLEMS

The test system we use in the present paper is designed to cover typical unsteady shocked flow features as fully as possible and includes shock waves, rarefactions, and contact discontinuities of different intensities and velocities as well as discontinuities at both sides of which the gas dynamic parameters vary in space. Although any test system has its own shortcomings and in principle cannot cover all possible situations, our previous experience suggests that a scheme performing well simultaneuosly for all below test problems may be recommended for practical usage with confidence.

First, we consider a few Riemann problems. The first one (test 480 : 1) has the pressure ratio $p_2/p_1 = 480$ and density ratio $\rho_2/\rho_1 = 8$. The gas with the specific heat ratio $\gamma = 5/3$ is at rest ($u_2 = u_1 = 0$) at the initial time moment $t_0 = 0$. The computation is carried out to $t_1 = 0.04$. It is a rather "tough," undeservedly forgotten test problem used by Boris and Book ([24]) and involving "strong" flow features.

The second Riemann problem (test 2 : 1) has the following parameters: $p_2/p_1 = 2$, $\rho_2/\rho_1 = 1$, $u_2 = u_1 = 0$, $\gamma = 1.4$, $t_1 = 0.25$. The test targets a scheme's performance for weak/moderate intensities of discontinuities and rarefactions as well as for slowly moving contact discontinuities. In fact, this is a modified version of the well-known Lax test. The modification is done in such a way that it slows down the contact discontinuity. As a result, the test immediately and clearly reveals any weakness a scheme may have in resolving contact discontinuities.

The third problem is the Sod [25] problem, which is a very popular although not a particularly difficult test. The parameters at the left from the initial discontinuity are $p_2 = 1.0$, $\rho_2 = 1.0$, $u_2 = 0$; at the right they are $p_1 = 0.1$, $\rho_1 = 0.125$, $u_1 = 0$. The specific heat ratio $\gamma = 1.4$; we compute to $t_1 = 0.25$.

The last Riemann problem producing two rarefaction waves and a low pressure/density region between them (the so-called "vacuum" test) was taken from [5]. The initial pressure and density are the same everywhere: $p_2 = p_1 = 1.0$, $\rho_2 = \rho_1 = 0.4$. The initial velocitites are of opposite sign: $u_2 = -2.0$, $u_1 = 2.0$. The specific heat ratio $\gamma = 1.4$; we compute to $t_1 = 0.15$.

For all the above problems the initial position of the jump in parameters is at $x = 0.5$, while the computational domain extends from $x = 0.0$ to 1.0 and contains 100 grid cells.

In many problems, unlike in the above test cases, the gas dynamic parameters are not constant on both sides of discontinuities. To cover such practical situations we employ the test problem of two interacting blast waves proposed by Woodward and Colella (the Woodward and Colella test [26]). The initial conditions of the test for the vector of primitive variables $V = (\rho, u, p)$ are

$$V(x, 0) = \begin{cases} V_l & \text{if } 0.0 \le x \le 0.1, \\ V_m & \text{if } 0.1 \le x \le 0.9, \\ V_r & \text{if } 0.9 \le x \le 1.0, \end{cases}$$

with $\rho_l = \rho_m = \rho_r = 1$, $u_l = u_m = u_r = 0$, $p_l = 1000$, $p_m = 0.01$, $p_r = 100$. The boundaries at $x = 0.0$ and 1.0 are solid walls. The computation is performed to $t_1 = 0.038$ using 800 cells with $\gamma = 1.4$. The numerical solution based on 10,000 cells is considered to be the "exact" one.

All test cases are computed with the Courant number 0.8. The second-order computations employ the β-limiter: $L(a, b) = \max\{0, \min\{\beta a, b\}, \min\{a, \beta b\}\}$ when $b \ge 0$ and $L(a, b) = \min\{0, \max\{\beta a, b\}, \max\{a, \beta b\}\}$ when $b \le 0$, with $\beta = 1.5$.

APPENDIX B: PROOF OF THE STATEMENT IN SECTION 5.1

It is proven here that for a nonlinear scalar hyperbolic conservation law with a convex flux the numerical flux of the differential AW scheme fully coincides with that of the Godunov scheme.

The proof is based on case-by-case analysis of (25), (26), (20), and (22), keeping in mind that the flux F is convex. Indeed, if both wave speeds $(\partial F/\partial U)_{i-1}$ and $(\partial F/\partial U)_i$, are positive, then $D^L(\xi) = \min\{0, a(\xi)\} \equiv 0$ for $\xi \in [0, 1]$, $d = 0$, and $\xi^* = 0$, so that $F_{i-1/2} = F(U_{i-1})$. In contrast, if $(\partial F/\partial U)_{i-1}$ and $(\partial F/\partial U)_i$ are both negative, then $D^R(\xi) = \max\{0, a(\xi)\} \equiv 0$ for $\xi \in [0, 1]$, $d = 0$, and $\xi^* = 1$, so that $F_{i-1/2} = F(U_i)$. Due to the convex property of the flux F the above two cases can be unified as follows: $F_{i-1/2} = \min_{U_{i-1} \le U \le U_i} F(U)$ for $U_{i-1} < U_i$ and $F_{i-1/2} = \max_{U_{i-1} \ge U \ge U_i} F(U)$ for $U_{i-1} > U_i$.

At $(\partial F/\partial U)_{i-1} < 0 < (\partial F/\partial U)_i$ and $U_{i-1} < U_i$ (expansion fan), for $\xi \in [0, \xi_{\min})$ $D^R(\xi) \equiv 0$ and $D^L(\xi) \neq 0$, while for $\xi \in (\xi^{\min}, 1]$ $D^R(\xi) \neq 0$ and $D^L(\xi) \equiv 0$ ($\xi^{\min}$ is the minimum point of F where $\partial F/\partial U$ and both AW velocities equal zero). The equality of the integrals in (26) is only possible when they both equal 0, i.e., the dissipation coefficient d becomes zero, and $\xi^* = \xi^{\min}$, i.e., the intermediate state ξ^* coincides with the minimum point of F. Therefore, $F_{i-1/2} = F(\bar{U}(\xi^*)) = \min_{U_{i-1} \le U \le U_i} F(U)$.

The crucial case for which many approximate Riemann solvers differ from the Godunov flux (see [12]) is a shock wave at $(\partial F/\partial U)_{i-1} > 0 > (\partial F/\partial U)_i$ and $U_{i-1} > U_i$. In this case $D^R(\xi) \equiv 0$ and $D^L(\xi) \neq 0$ for $\xi \in (\xi^{\min}, 1]$ and $D^R(\xi) \neq 0$ and $D^L(\xi) \equiv 0$ for $\xi \in [0, \xi^{\min})$. The diffusion coefficient d may be then found using the following expression obtained from (26), (20), (22), and (16), taking into account the fact that $\xi^* \in [\xi^{\min}, 1]$ for $F_{i-1} \le F_i$ while $\xi^* \in [0, \xi^{\min}]$ for $F_{i-1} \ge F_i$:

$$
\begin{aligned}
d &= \frac{F(\bar{U}(\xi^*)) - \max\{F(U_{i-1}), F(U_i)\}}{U_i - U_{i-1}} \\
&= \frac{\min_{U_i < U < U_{i-1}} F(U) - \min\{F(U_{i-1}), F(U_i)\}}{U_i - U_{i-1}}.
\end{aligned} \tag{B.1}
$$

The resulting flux is $F_{i-1/2} = \max\{F(U_{i-1}), F(U_i)\} = \max_{U_{i-1} \ge U \ge U_i} F(U)$.

The most interesting point is that in this case the intermediate state ξ^* appears to be different from the state at the face in the Godunov scheme obtained from the exact solution of the Riemann problem. Nevertheless, the total numerical flux (25) consisting of the flux at the intermediate state $F(\bar{U}(\xi^*))$ and the numerical dissipation term d just determined as (B.1) coincides with that of the Godunov scheme, as for all other cases considered here.

ACKNOWLEDGMENT

Prof. P.A. Voinovich read preliminary versions of the paper and made many valuable suggestions on notations. His general interest and encouragement are also appreciated.

REFERENCES

1. M. Brio and C. C. Wu, An upwind differencing scheme for the equations of ideal magnetohydrodynamics, *J. Comput. Phys.* **75**, 400 (1988).
2. A. Harten, P. D. Lax, and B. van Leer, On upstream differencing and Godunov-type schemes for hyperbolic conservation laws, *SIAM Rev.* **25**, 35 (1983).
3. B. Einfeldt, On Godunov-type methods for gas dynamics, *SIAM J. Numer. Anal.* **25**, 294 (1988).
4. B. Einfeldt, C. D. Munz, P. L. Roe, and B. Sjögreen, On Godunov-type methods near low densities. *J. Comput. Phys.* **92**, 273 (1991).
5. E. F. Toro, *Riemann Solvers and Numerical Methods for Fluid Dynamics*, 2nd ed. (Springer-Verlag, New York, 1999).

6. I. V. Sokolov, J. Sakai, and E. V. Timofeev, On high-resolution shock-capturing schemes for hydrodynamic and MHD simulations via an artificial wind concept, in *Proceedings of the 12th National CFD Symposium, Chuo University, Tokyo, Japan, December 21–23, 1998*, pp. 93–94.
7. I. V. Sokolov, E. V. Timofeev, J. Sakai, and K. Takayama, On shock-capturing schemes using artificial wind, *Shock Waves J.* **9**, 423 (1999).
8. H. M. Zhang, I. V. Sokolov, and J. Sakai, Towards easy and efficient computational relativistic hydrodynamics, submitted for publication.
9. W. J. Rider, A review of approximate Riemann solvers with Godunov's method in Lagrangian coordinates, *Comput. Fluids* **23**, 397 (1994).
10. I. V. Sokolov, E. V. Timofeev, J. Sakai, and K. Takayama, Development and applications of artificial wind schemes for hydrodynamics, MHD and relativistic hydrodynamics, in *CD-ROM Proceedings of the 13th National CFD Symposium, Chuo University, Tokyo, Japan, December 21–23, 1999*, paper Nr. E1-05.
11. E. V. Timofeev, I. V. Sokolov, J. Sakai, and K. Takayma, On the artificial wind schemes, *Rep. Inst. Fluid Sci. Tohoku Univ.* **12**, 71 (2000).
12. C. Hirsch, *Numerical Computation of Internal and External Flows* (Wiley, New York, 1990), Vol. 2.
13. A. V. Rodionov, Increasing of approximation order of the Godunov scheme. *Zh. Vychisl. Mat. Mat. Fiz. (J. Comput. Math. Math. Phys.)*, **27**(12), 1853 (1987), in Russian.
14. T. Saito, P. Voinovich, E. Timofeev, and K. Takayama, Development and application of high-resolution adaptive numerical techniques in Shock Wave Research Center, in *Godunov methods: Theory and Applications*, edited by E. F. Toro (Kluwer Academic/Plenum Publishers, New York, 2001), p. 763.
15. P. A. Voinovich, *Two-Dimensional Locally Adaptive Unstructured Euler Code*, Report of the Advanced Technology Center, St. Petersburg, Russia (1993).
16. E. V. Timofeev, K. Takayama, and P. Voinovich, *Numerical and Experimental Observation of Three-Dimensional Unsteady Shock Wave Structures*, AIAA Paper 97-0070 (1997).
17. K. Takayama and O. Inoue, Shock wave diffraction over a 90 degree sharp corner—Posters presented at 18th ISSW, *Shock Waves* **1**, 301 (1991).
18. E. V. Timofeev, P. A. Voinovich, N. Nagayashi, K. Takayama, I. V. Sokolov, and J. Sakai, Artificial wind schemes as simple and efficient tool to simulate diverse shock wave flows, in *CD-ROM Proceedings of the 23rd Int. Symp. on Shock Waves, Fort Worth, USA, 23–27 July, 2001*, edited by F. Lu (The University of Texas, Arlington, 2002).
19. E. Timofeev, P. Voinovich, and K. Takayama, On underwater shock wave propagation induced in the World Ocean by impact of a celestial body, in *SCFS'2000*, *Proceedings of the Symp. on Computational Fluid Science, Institute of Fluid Science, Tohoku University, Sendai, Japan, August 23, 2000*, edited by T. Ikohagi, IFS-TM011 (Institute of Fluid Science, Tohoku University, Sendai, Japan, 2000), pp. 67–74.
20. I. V. Sokolov and J. Sakai, Strong magnetic implosion in spherical reversed laser corona: New results and new numerical schemes for MHD simulations, *J. Plasma Fusion Res. Ser.* **2**, 482 (1998).
21. H. M. Zhang, I. V. Sokolov, and J.-I. Sakai, Oscillations, shocks and fine wave structures arising during the coalescence of two force-free current loops, *Plasma Phys. Rep.* **27**(4), 303 (2001).
22. J.-I. Sakai, A. Takahata, and I. V. Sokolov, Heating of coronal loop footpoints by magnetic reconnection resulting from surface Alfvén waves and colliding plasma flows in chromospheric current sheets, *Astrophys. J.* **556**, 905 (2001).
23. H. M. Zhang, I. V. Sokolov, K. Furusawa, and J.-I. Sakai, Applications of artificial wind numerical scheme for relativistic hydrodynamics in astrophysics, *Prog. Theor. Phys. Suppl.* **138**, 642 (2000).
24. J. P. Boris and D. L. Book, Flux-corrected transport. I. SHASTA, a fluid transport algorithm that works, *J. Comput. Phys.* **11**, 38 (1973).
25. G. A. Sod, A survey of several finite-difference methods for systems of nonlinear hyperbolic conservation laws, *J. Comput. Phys.* **27**, 1 (1978).
26. P. Woodward and P. Colella, The numerical simulation of two-dimensional flows with strong shocks, *J. Comput. Phys.* **54**, 115 (1984).